AD 407 917

THE JOHNS HOPKINS UNIVERSITY
CARLYLE BARTON LABORATORY
BALTIMORE, MARYLAND

Technical Report No. AF-104

A FORMING STUDY OF POINT-CONTACT TUNNEL DIODES

by

H. J. Lory

Program Element Code: 62405454
Technical Area: 760D
Task: 403601

Project Engineer:

1/Lt. W. F. H. Ring, Extension 33222
Aeronautical Systems Division
Wright-Patterson Air Force Base, Ohio

Contract No. AF 33(657)-11029
(Formerly AF 33(616)-6753)

May 1963

THE JOHNS HOPKINS UNIVERSITY
CARLYLE BARTON LABORATORY
BALTIMORE, MARYLAND

Technical Report No. AF-104

A FORMING STUDY OF POINT-CONTACT TUNNEL DIODES

by

H. J. Lory

Program Element Code: 62405454
Technical Area: 760D
Task: 403601

Project Engineer:

1/Lt. W. F. H. Ring, Extension 33222
Aeronautical Systems Division
Wright-Patterson Air Force Base, Ohio

Contract No. AF 33(657)-11029
(Formerly AF 33(616)-6753)

May 1963

TABLE OF CONTENTS

LIST OF ILLUSTRATIONS

ACKNOWLEDGMENTS

I am indebted to Dr. Ralph Tramburulo of Bell Telephone Laboratories for the suggestion which initiated this work.

Mr. Francis Trageser was of considerable assistance in preparing samples and building the necessary instruments.

Miss Phyllis Shipley assisted in some of the numerical calculations.

The first referee was Dr. C. F. Miller; the second was Dr. P. E. Wagner.

Mrs. Dolores Scholl typed both the preliminary drafts and the final copy of the dissertation.

This work was supported by the Air Force Systems Command, United States Air Force.

In addition to the foregoing, there were numerous other individuals to whom I am indebted for advice, materials, and assistance. Unfortunately, it would not be practical to enumerate them all here.

ABSTRACT

The factors involved in the forming of point-contact tunnel diodes by the application of brief electrical overloads are studied. As a test of the theory, a diode fabricated from N-doped germanium and an aluminum catwhisker is used through the paper.

After a brief review of the thermal and electrical conductivities of heavily doped germanium at elevated temperatures, an evaluation is made of the critical breakdown voltage (the applied voltage below which no forming of any type occurs), assuming constant electrical and temperature-dependent thermal conductivity.

Junction effects are taken into account by considering the "cold" diode characteristic in predicting a voltage below which current is limited by junction effects and above which spreading resistance dominates. This yields a value of series voltage which must be subtracted from the applied pulse voltage in calculating an effective critical voltage. The critical voltage for the sample diode is calculated and the result agrees well with experiment.

For voltages higher than the critical voltage, it is assumed that a eutectic region is formed under the point, extending into the body of the semiconductor. The extent of this region is computed, taking into account thermoelectric effects. On the basis of this a thermal time constant is computed which agrees well with experiment.

A heat flow pattern is computed, and, on the basis of this, two different types of diode structures emerge. The first is characterized by a metal-semiconductor interface lying in the original plane of the semiconductor; this configuration does not lead to expitaxial regrowth of germanium onto the original lattice and exhibits a typical metal-semiconductor I-V characteristic. The second, which corresponds to heavy forming, is characterized by a eutectic region extending deep into the body of the semiconductor; here the heat flow pattern is such that regrowth of a single crystal P-N junction is to be expected, a situation which leads to the formation of tunnel diodes.

In a typical example, solid-state diffusion is found to be negligible.

I. INTRODUCTION

The object of the present paper is to investigate the processes involved when a point-contact tunnel diode is "formed" by the application of a short electrical overload.

Forming techniques used in diodes and transistors have, for the most part, been derived by trial and error, principally because of the complicated nature of the problem. One of the most rigorous treatments in the literature is that of A. C. Sim (1). Sim solved the Maxwell's equations and the heat flow (with source) equation, making a number of assumptions primarily valid for a diode of the type commonly used for detectors, harmonic generators and the like. He assumed that the semiconductor material was nearly intrinsic, that the point material was more refactory than the semiconductor and that "thermal" impurity states (presumably due to indiffused copper atoms or lattice dislocations) are the primary cause of the formation of a P-N junction in the neighborhood of the contact.

None of these assumptions are entirely valid in the present case. With the heavily doped materials used in tunnel diodes, the extrinsic conductivity cannot be ignored, at least at the lower temperatures, and the point materials often melt at temperatures low compared to semiconductor melting points. The P-N junction is formed by indiffusion of dopants contained in the wire, these dopants ordinarily being column III and V elements in the case of the

elemental semiconductors and column II-VI elements for the covalent semiconductors. Sim came to several conclusions as a result of his analysis, one of which was the desirability of a high-impedance pulse supply. Burris and Tramburolo (2), as well as the author, on the other hand, have found that even for relatively low-current units, a pulse supply having an internal impedance of an ohm or less was usually necessary.

Torrey and Whitmer (3) made important contributions to the knowledge of the fields and thermal gradients in point contact diodes in the course of their investigation of breakdown in detector diodes due to T-R tube leakage. Since they were primarily interested in catastrophic effects, they did not delve into resulting structures, however.

There was a reawakening of interest in the problem with the advent of the point contact transistor, due to observed improvements in performance when the collector was subjected to forming pulses. A number of papers were written discussing this phenomena, most of the work being either experimental results or theoretical work of a qualitative nature (5, 6, 7). This, however, was only a temporary interest, as the point-contact transistor declined in importance as junction - transistor performance rapidly improved.

There has been considerable interest (5, 8, 9) shown from time to time in the influence of surface effects on formed point contacts, a subject which we shall neglect on the assumption that

such effects are of relatively small significance in a low-impedance device such as a tunnel diode.

Most of the work in tunnel diodes has centered about diodes fabricated using dot-alloy techniques (10, 11, 12). In these devices, the frequency of cutoff may be increased by decreasing the junction area, since the spreading resistence increases inversely as the contact radius, while the junction capacity varies as the square of this radius. While there are techniques for reducing the size of the contact area in alloy junctions, it is difficult to achieve in this manner areas as small as those easily obtainable using a point-contact configuration. Burris and Tramburolo have done considerable work with the point contact configuration, and have reported fundamental oscillations at 103 KMc (2, 13, 14). Burris and Tramburolo have found a wide variation in the forming techniques necessary to form the diode properly.

The problem is an exceedingly complex one, involving at many points effects which are rather poorly understood at the present time. For this reason, the present paper will not attempt to cover the topic in full generality. Instead, an attempt will be made to take a particular metal-semiconductor combination and treat it theoretically and experimentally, it being anticipated that some of the results so obtained might serve at least as starting points in the analysis of other combinations.

The wire chosen is aluminum. The use of aluminum avoids the difficulty arising in the use of solvents such as tin or lead, namely that of finding and interpreting phase diagrams relating to three elements. In order to render the aluminum relatively easy to work, 1% of Boron was added. The effects of this small addition will be considered later.

The semiconductor chosen was germanium, since there is probably more tabulated data related to it than to any other semicondutor. The germanium was doped to 3×10^{19} aresnic atoms/cc, it being difficult to pull reasonably uniform single crystals at higher doping levels.

In this paper, the experimental and theoretical work will be presented simultaneously, since the numerous approximations involved require justification before proceeding to extension of the theory built upon these approximations.

In order to carry through an analysis of the electrical and thermal effects in the neighborhood of a point contact, it is necessary to have some notion of the manner in which the electrical and thermal conductivities of the heavily doped material varies with temperature, especially at high temperatures. Consequently, Section II will be devoted to a review of the theoretical and experimental estimates of the thermal and electrical conductivity of heavily n-doped germanium in the region between room temperature and the melting point of germanium.

The range of voltages ordinarily used in forming the diodes is such that junction effects may be reasonably expected to play a part in limiting the current. For this reason, Part III will be devoted to a theoretical review and experimental study of the forward and reverse I-V Characteristics of the diode.

It appears that there exists a critical pulse voltage, below which the parameters of the diode undergo no change; this obviously must be the case if the diode is to function at all. In Section IV this critical voltage will be calculated and the theoretical predictions checked experimentally.

In Section V the thermal profile of the diode for pulse voltages greater than the critical voltage is calculated. Estimates are made on the thermal time constant.

It is of some practical importance to be able to control the current level of the finished diode. The factors involved in this are discussed in Section VI together with relevent experiment results.

In Section VII the information obtained in Section V is used to calculate the impurity profile in the finished diode. This may then be compared to experimental results.

Section VIII will be a review of the preceding material as well as a short discussion of some of the factors omitted in the treatment.

II. TRANSPORT PROCESSES IN HEAVILY DOPED SEMICONDUCTORS

A. Thermal Conductivity

In this section we shall discuss the thermal conductivity of semiconductors in general and germanium in particular.

Figure 1 shows the results of thermal conductivity measurements carried out by Abeles (15) and Slack and Glassbrenner (16). Abeles used a longitudinal heat-flow apparatus, while Slack and Glassbrenner used a radial flow configuration, in which a heating wire ran through the center of the sample and the thermocouples were placed radially out from the center. This latter method has the advantage that, aside from negligible end effects, radiated heat need not be taken into account; for this reason, it probably yields the more reliable data. Unfortunately, this method was used only on intrinsic material. Abeles, however, measured conductivities for heavily doped materials (0.001 ohm-cm). At low temperatures these conductivities coincide with his own measurements for intrinsic material, while at high temperatures they lie between his intrinsic measurements and those of Slack and Glassbrenner.

The general picture for both doped and undoped material seems to be a region of $T^{-1.2}$ dependence from 300°K to around 900°K, followed by an abrupt upswing.

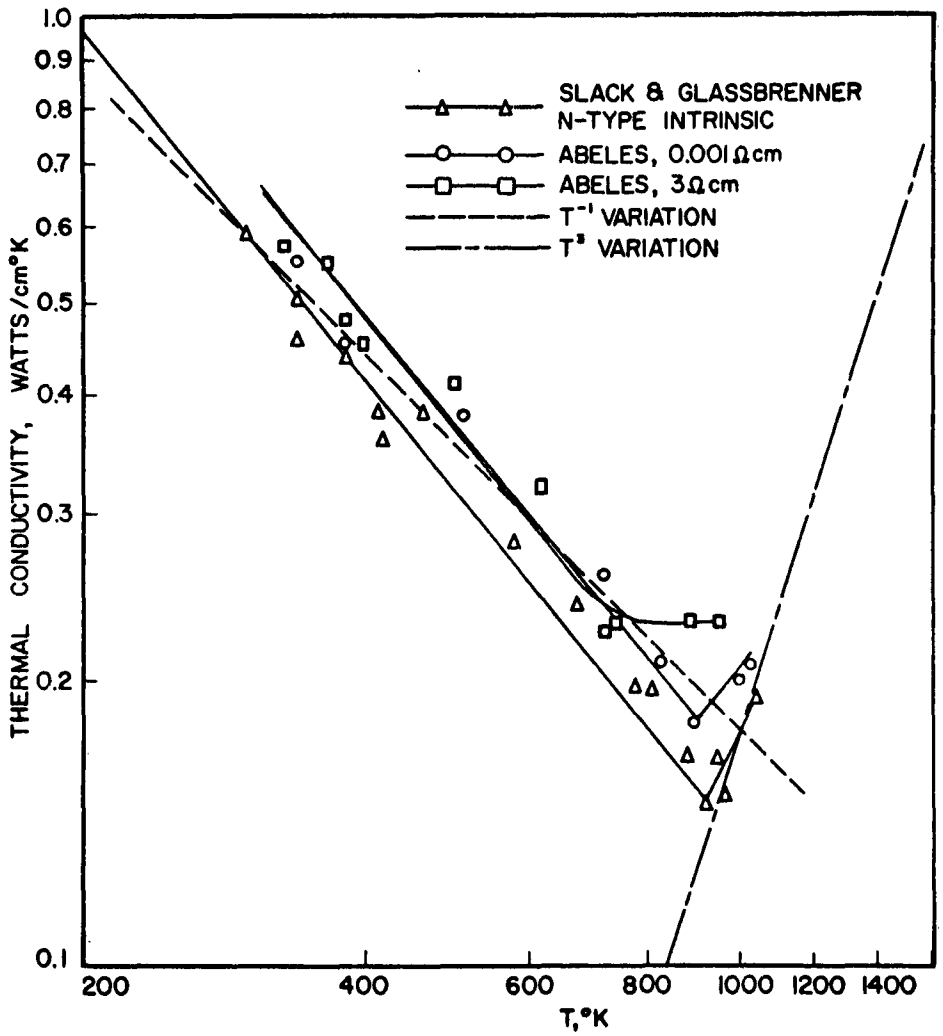

FIGURE 1 THERMAL CONDUCTIVITY OF GERMANIUM AS A FUNCTION OF TEMPERATURE.

The following discussion is not intended to be a tutorial section on thermal conductivity; such would be beyond the scope of the paper. Rather, it is intended to serve as a guide to any extrapolations which might be necessary in applying the rather meagre experimental data to other forming problems.

The most important concept to grasp in considering thermal conduction in a semiconductor is that of phonon scattering. If we consider a crystal to be perfectly uniform, and if we assume that the forces binding the atoms together vary linearly with the atomic displacement from the lattice site, and if we further postulate a particularly convenient type of cyclic boundry condition, it is possible to solve the equations of motion for the atoms in the crystal by deriving a set of normal coordinates (17, 18, 19). When our equations of motion are written in terms of these new coordinates, they resemble a set of equations for G independent three-dimensional oscillators, where G is the number of unit cells in the crystal. The normal coordinates are identified by a wave number $\vec{k}$. The displacements of the atoms in the lattice may be written in terms of $\vec{k}$, in such a manner that they resemble a superposition of traveling waves. (see Equation (1)).

$$U(x) = \frac{1}{\sqrt{G}} \sum \mathcal{e}_j \, b_j(\vec{k}) \exp i\vec{k} \cdot \vec{x} + i\omega_j(\vec{k})\, t \qquad (1)$$

The vibrational energy of the crystal is equal to the sum of the energies of the independent oscillators. Quantum mechanical considerations require that the energy of each of the independent oscillators must be an integer multiple of $h\omega$, where ω is the angular frequency of oscillation of the oscillator. Moreover, it is possible to superimpose modes whose wave vectors lie within a range $\Delta\vec{k}$. This will give rise to a packet of spatial extent $\Delta\vec{x} \sim \Delta\vec{k}$. This localized packet is called a phonon.

The phonons carry a heat current proportional to their number N, energy $h\omega$, and group velocity $\frac{\partial\omega}{\partial k}$:

$$Q = \sum_{\vec{k}} N(\vec{k})\, h\omega\, \frac{\partial\omega}{\partial k} \quad . \qquad (2)$$

A study of Equation (2) indicates that, if the distribution of modes in $\vec{k}$ space is symmetrical, there will be no heat flow. Moreover, if there is an asymmetry in the distribution an no mechanism for removing the asymmetry, there will be a constant flow of heat. Since this is equivalent to an infinite conductivity, there must be mechanisms tending to redistribute energy among the phonons in such a way as to make N symmetric in $\vec{k}$.

Our initial formulation left no possibility for the interchange of energy among the phonons, so that, in order to arrive at a finite conductivity, it is necessary to consider a less ideal model. There are three possible approaches:

1. A reconsideration of the boundary conditions might be made, replacing the mathematically convenient by physically unrealistic cyclic conditions with more a precise representation of the boundaries.

2. A relaxation in the original requirement that the crystal be perfect. Thus, the presence of vacancies, interstitials, substitutional impurities, faults, conduction electrons, and other deviations from perfect periodicity could cause a scattering of a phonon, with a consequent variation in the distribution of phonon energies.

3. A consideration of the possibility that the restoring forces acting on the atom are not proportional to displacement.

Boundary effects have been shown to be negligible down to liquid helium temperatures (20).

In considering other types of scattering by stationary defects, we must divide the temperature range into two parts, the dividing point being θ_D, the Debye temperature. The Debye temperature is derived by considering a solid to be a continuum and taking its atomic nature into account by limiting the possible number of lattice vibrational modes to three times the number of atoms in the crystal. If we call this highest permitted frequency γ_D, the θ_D is defined by Equation (3).

$$\theta_D = \frac{h\gamma_D}{K} \qquad (3)$$

where K is Boltzmann's constant. θ_D is the point at which the lattice heat capacity begins to level out (See Figure 2). According to Klemens (17), the portion of the thermal resistance due to the scattering of lattice waves by static impurities varies with T below the Debye temperature and is constant above. This may be seen by referring to Figure 2 and writing the thermal conductivity in the form shown in Equation (4)

$$K = \frac{1}{3} \int S(\omega)\, L(\omega)\, d\omega \qquad (4)$$

where $S(\omega)$ is the specific heat per unit frequency interval. Since the net specific heat is found to be integrating $S(\omega)$ does not appear unreasonable that there should be a correlation between S(T) and K(T).

For our purposes, this dependence of K on T^1 below the Debye temperature and T^0 above θ_D means that it is possible to evaluate the importance of point impurity scattering by evaluating the room temperature thermal conductivity of our highly doped material and comparing it to that of instrinsic material: if there is no difference at room temperature, one may safely ignore point-impurity scattering at higher temperatures. Klemens (21) has also shown what intuitively seems clear: that, when substitutional impurities are randomly distributed (an assumption ordinarily made with dopants), their contribution to thermal resistance varies as the impurity density. Since according to the resistivity data of Trumbore and Tartaglia (22), the material used in our example has an impurity density of only two or three times that of the degenerate samples of Abeles (15),

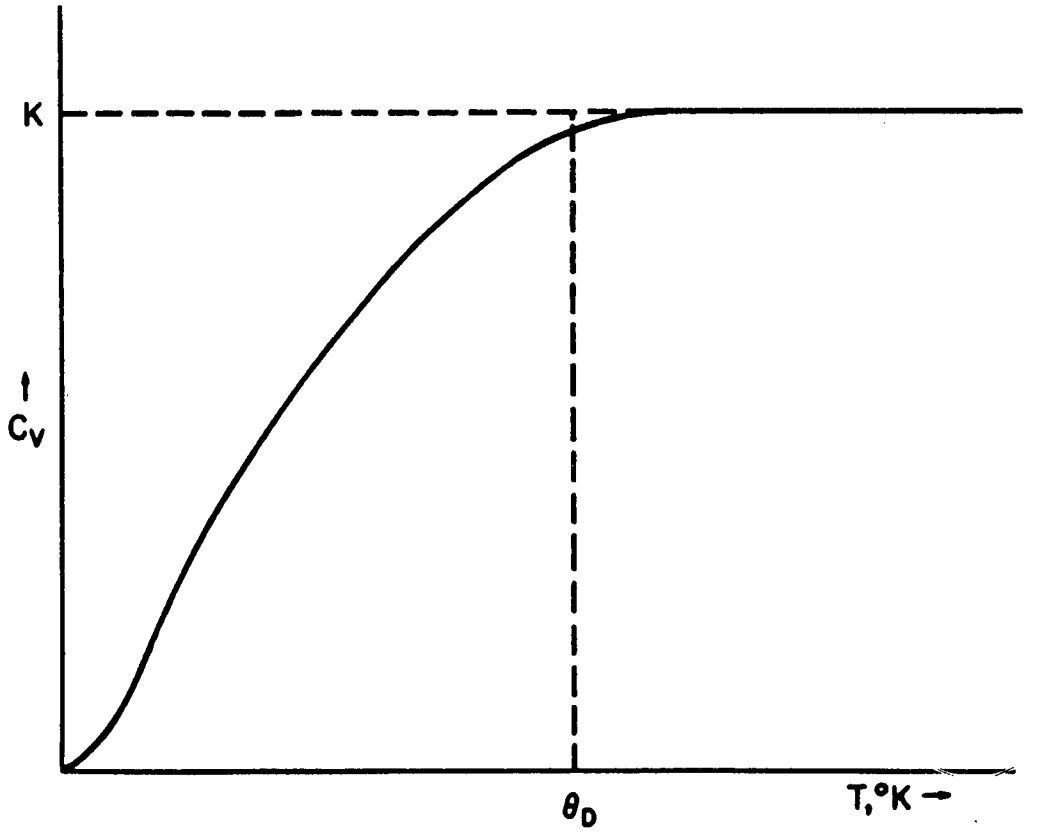

FIGURE 2 SPECIFIC HEAT OF TYPICAL SOLID.

and since the data of Abeles shows no indication of point impurity scattering, we may also assume that this may be neglected in our case.

The third effect mentioned, that of non-linear restoring forces on the atoms, is the most important one (at least in the case of germanium and silicon) over a wide range of temperatures. The theory is rather complicated, and has been worked out in detail by Klemens (17); in brief the non-quadratic energy terms arising from the nonlinear restoring forces give rise to interactions between three different vibrational modes. This is called a three-phonon collision, and can occur in two different ways. If the collision conserves crystal momentum $h\vec{k}$ it is called a normal of N-process; if it only conserves momentum to within a vector of the reciprocal lattice, it is called an umklapp or U-process. The U-processes are the ones which contribute directly to thermal conductivity. At temperatures above θ_D umklapp processes lead to a T^{-1} dependence of thermal conductivity, shown in Figure (1) fitted to room temperature thermal conductivity. There does not seem to be any universally accepted explanation for the difference between the experimental $T^{-1.2}$ variation and the theoretical T^{-1} variation.

In casting about for an explanation for the increase in thermal conductivity starting around $940^{o}K$, perhaps the first thing that might occur to one is that the conduction electrons supplied by

the heavy dopant concentration might be carrying an appreciable amount of heat. The contribution of the conduction electrons to thermal conductivity is a familiar problem whose solution, the Wiedeman-Franz law (23), may be expressed as Equation (5)

$$Ke = 2\sigma T \left(\frac{k}{e}\right)^2 \quad . \qquad (5)$$

σ is the electrical conductivity at temperature T. To estimate the importance of the electronic thermal conductivity, suppose that we are dealing with material of 3000 ohm^{-1} cm^{-1} conductivity, which is about as degenerate as is commonly in use for these diodes. Then, assuming that the electrical conductivity does not increase as the temperature is raised, we get an electronic thermal conductivity at 1200°K of 5.5×10^{-2} watts/cm deg, which is negligible compared to the extrapolated value of the phonon scattering contributions to the thermal conductivity.

Price (24, 25) has investigated another carrier effect influencing the thermal conductivity of semiconductors. The carriers involved are intrinsic, thermally dissociated electron-hole pairs whose concentration varies with temperature. Thus, thermal gradients give rise to diffusion currents, in which each hole or electron carries with it an amount of energy equal to the forbidden energy gap width. Slack and Glassbrenner (16) have computed the contribution to the thermal conductivity using Prices formula and the data of Morin and Miata (26) and MacFarlane et al (27). Their prediction for the thermal conductivity for intrinsic germanium at

the higher temperatures is a T^3 dependence and a thermal conductivity of 0.1 watt/cm deg, which is extremely close to the extrapolated experimental data.

The question arises as to the extension of these results to heavily doped material. The only manner in which heavy doping could enter into the ambipolar diffusion process would be to decrease the electron and hole mobility by the addition of an impurity scattering process. The degree to which impurity scattering effects the mobility decreases with increasing temperature and there is some data (28) available which seems to suggest that, even at these high dopings, the presence of impurities does not greatly effect the mobilities in the temperature range 900-1200^{o}K.

We may then represent the conductivity of germanium of all doping levels by Figure 3. The fact that we may, at least in an approximate treatment, neglect the effects of doping in considering thermal conductivity at the temperatures in which we are interested simplifies the problem significantly. The actual dopant level in the semiconductor is not uniform during certain stages of the forming process; the doping is a function of the temperature, and if the thermal conductivity were a function of the doping, the problem would become hopelessly complicated.

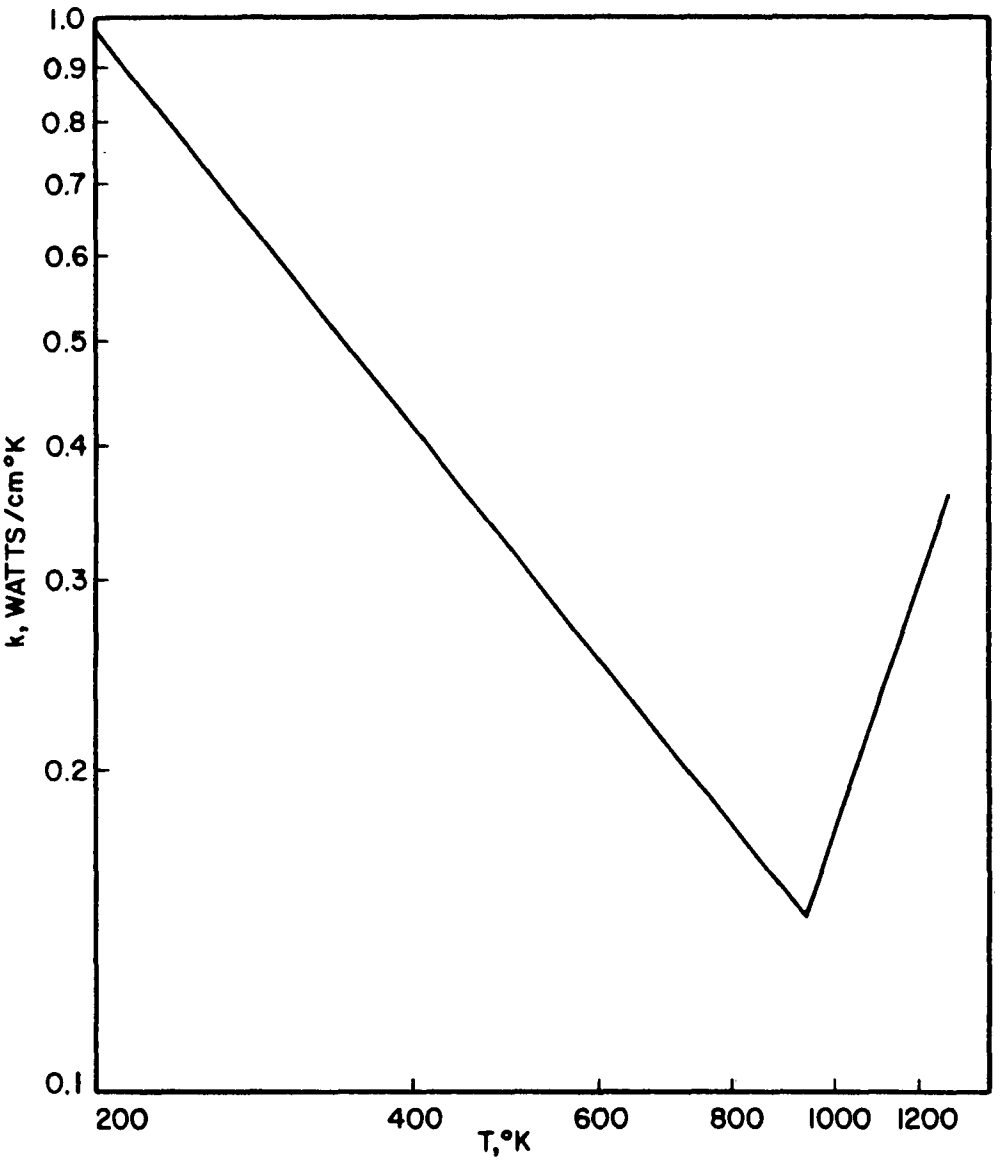

FIGURE 3 THERMAL CONDUCTIVITY OF GERMANIUM AS A FUNCTION OF TEMPERATURE.

B. Electrical Conductivity

Unfortunately for the present purpose, there seems to be very little in the literature concerning the conductivity of degenerate semiconductors as a function of temperature. The present section will discuss the theory known to be applicable to more highly doped semiconductors and attempt to justify the assumption that the temperature coefficient of resistivity of our degenerate semiconductors may be ignored for the present purpose.

We shall consider variations of carrier density and mobility separately. The situation with respect to carrier density is simple, so we shall consider it first. At relatively low temperatures (between about 300° and 1000°K) essentially all of the conduction electrons are supplied by the ionization of impurity atoms, provided that the material is doped to degeneracy. There is a considerable body of experimental evidence (22, 10, 29, 32) to indicate that, at room temperature, in semiconductors doped to levels higher than 10^{18} carriers/cc., the activation energy vanishes, and the donors are completely ionized. Hence we may assume a 1:1 relationship between electrically active impurity atoms and conduction electrons up to the temperatures where excitation from the valence bonds becomes important. It might be pointed out that the term "electrically active" is used here to avoid consideration of occluded GeAs clusters which sometimes occur in heavily doped germanium (30).

At higher temperatures, the electrons excited up into the conduction band from the valence band become important. In a rigorous treatment, one would have to consider the effect of the doping in order to calculate the intrinsic electron density, since the Fermi level is determined by both impurity and intrinsic electron density. However, the error in the Fermi level resulting from temporarily ignoring impurity electrons is not sufficient to greatly effect the results. A Semi-empirical computation of the intrinsic electron distribution was carried out by Morin and Maita (26), working backward from intrinsic conductivity measurements of Debye and Conwell (32) and the theoretical mobility dependence found by Morin (33). Combining this with extrinsic carrier concentration yields a concentration variation of the form shown in Figure 4. For our purposes it is clear that variation of total carrier density will have virtually no effect on the resistivity.

The variation of mobility is a considerably more complex subject than that of carrier concentration variation. Unfortunately for our purposes, there seems to be very little in the literature regarding high-temperature electrical conductivity in degenerate semiconductors. The two most important scattering mechanisms are lattice vibrational scattering and impurity scattering.

The former has been studied by Bardeen and Shockly (34, 35), who took as their model of a band structure that of the unperturbed lattice, plus perturbations representing the thermal vibrations.

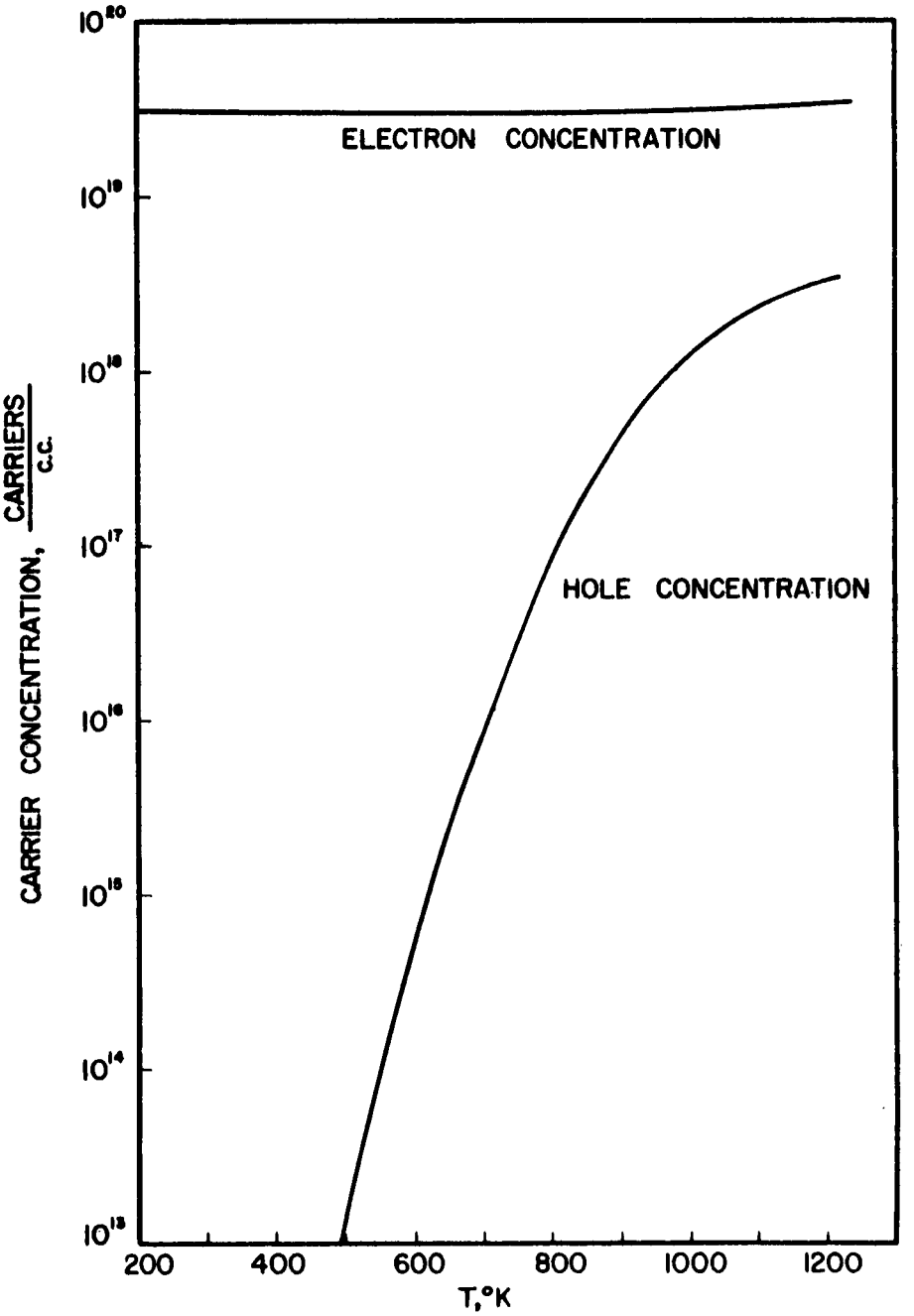

FIGURE 4 HOLE AND ELECTRON CONCENTRATIONS VERSUS T. $N_D = 3 \times 10^{19}$ $\frac{\text{carriers}}{\text{cc}}$.

After analysing the resulting scattering, Bardeen and Shockley predicted a $T^{-1.5}$ dependence of intrinsic mobility on temperature. Experimental results (31), however, indicate a temperature dependence of $T^{-1.66}$ for electron mobility and $T^{-2.33}$ for hole mobility. The reason for the discrepancy is not clear; it has been suggested (31) that the many-valley characteristic of E(K) may explain the anomoly. Figure 5 shows μ_L, the lattice mobility contribution, plotted against T.

The basic treatment of scattering by ionized impurities was carried out by Conwell and Weisskopf (36), using a model similar to that used for Rutherford scattering. Subsequent studies (32, 37, 38) have been mostly refinements of this work. The Conwell-Weisskopf formula for the ionized impurity scattering contribution to the resistance is given by Equation (6)

$$\mu_I = \frac{2^{7/2} k^2 \epsilon_o^2 (KT)^{3/2}}{\pi^{3/2} m_n^{1/2} e^3 N_I \mathrm{Ln}\left[1 + \left(\frac{3k\epsilon_o KT}{e^2 N_I^{1/2}}\right)^2\right]} . \qquad (6)$$

A plot of μ_I versus T for the case of germanium doped to 3×10^{19} carriers/c.c. is given in Figure 5. Also given is a composite mobility using a combination formula of Johnson and Lark-Horovitz (39).

The Conwell-Weisskopf formula is essentially a classically derived expression. Brooks (41) attacked the problem from a

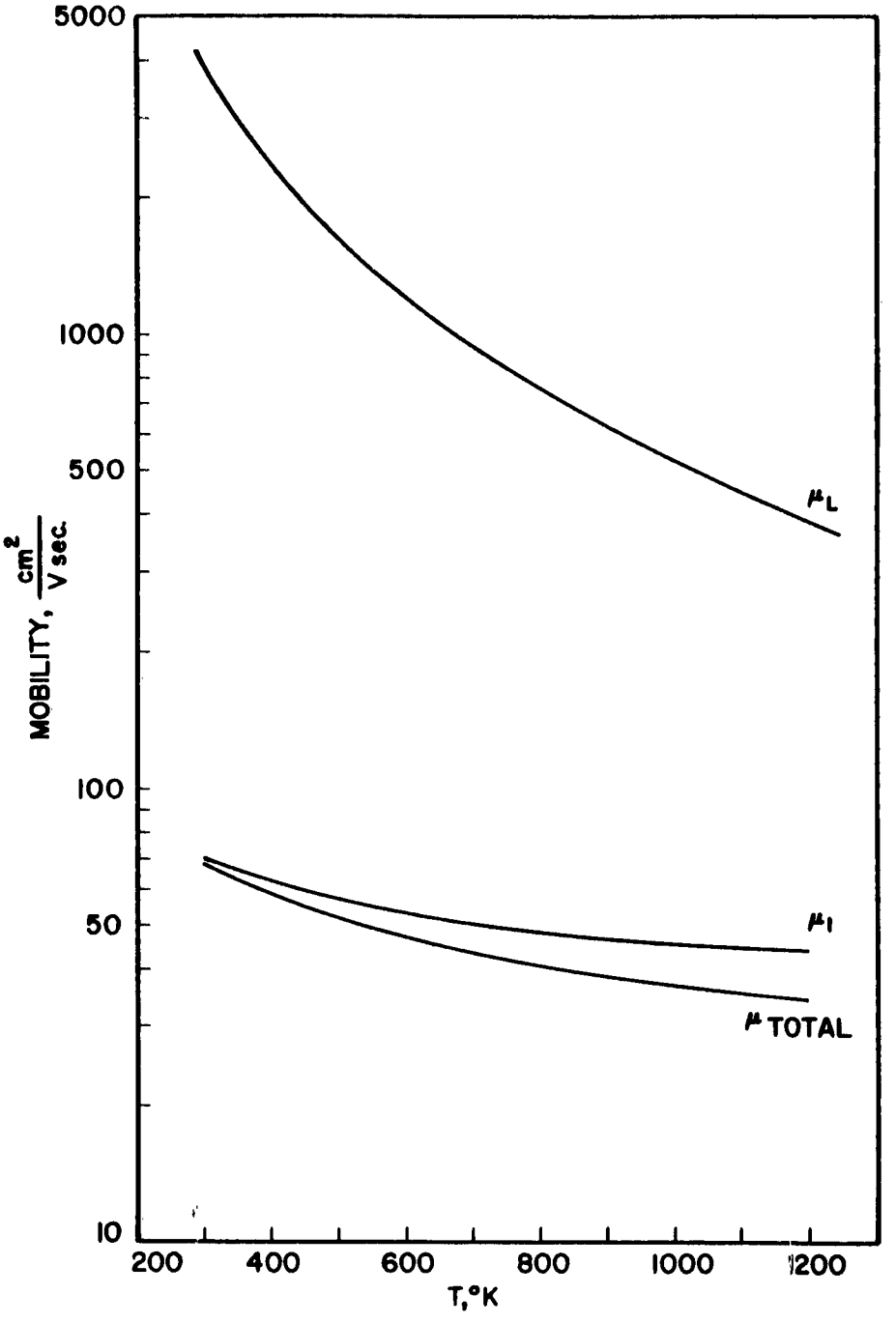

FIGURE 5 ELECTRON MOBILITY VERSUS T.

quantum-mechanical point of view and concluded that Equation (6) should have a multiplication factor of $\frac{me^2}{N^{1/3}T\pi K^3}$ in the argument of the logarithmic term. Although the meaning of K is not clear, which precludes numerical correction of the Conwell-Weisskopf expression, it is clear that by suppressing the denominator, the correction tends to prevent the decrease of μ with increasing temperature. This is what we expect, since, by using the Fermi statistics instead of Boltzmann statistics, one considers only those electrons having energies around the Fermi energy, which in germanium is only weakly dependent on temperature. Hence thermally induced variations in energy in the "tails" of the distribution have relatively little effect on the mobility. Now, even with the pessimistic Conwell-Weisskopf prediction, the mobility and hence the conductivity varies only a factor of two between room temperature and the melting point. In view of our expectation that the variation is even less, we shall make the assumption that the resistivity is a constant.

This assumption is crucial to the analysis. Without it, it would be necessary to solve the thermal and electrical equations simultaneously, each equation involving nonlinear functions of the solution of the other. By assuming that the temperature coefficient of resistivity may be justifiably ignored, one may solve first the Maxwell equation for potential or current distribution, then the

thermal conductivity equation, using the solution to the former as sources in the latter.

C. Thermoelectric Effects

Although they are classified as transport processes, we shall defer the discussion of thermoelectric effects until Section V.

III. JUNCTION EFFECTS

The purpose of this section is to derive a model of the diode which will permit computations which take into account junction effects.

Two points should be made here. In all our studies we shall assume that the point is given a very light current pulse to anchor it to the semiconductor before the main forming pulse is applied; otherwise, there would have been too much mechanical instability, and surface effects might have played an excessive part in the starting conditions. Secondly, most of our experiments were conducted with cleaved surfaces, with surfaces ground and etched with CP_4, and with surfaces ground and etched with hydrogen peroxide etch. The principal difference in results was that cleaved surfaces tended to permit more sensitive determination of contact as the wire was brought in to touch the semiconductor than was possible with etched surfaces. For a given wire, contact pressure, and forming system, the three types of surface preparation had little influence in the final diode.

Since all our successful tunnel diodes were made using forward pulses, we shall consider the forward characteristic first. By and large, we may consider the forward characteristic as being divided into three distinct regions; the first dominated by the tunneling current, if any, the second by the normal diode current, and the third by the effects of spreading resistance.

Although the tunneling current plays no direct part in the forming process, we shall discuss it here in some detail, in order to derive some criterian for the impurity profile necessary to form a tunnel diode.

In the first place it must be realized that we are dealing here with a P-N junction formed by the alloying of the point materials and not with a metal-semiconductor junction. This fact has been established by thermoelectric probing experiments, (42) and by the fact that alloys suitable for dot-alloy metals also usually work well for point-contact wires.

The requirements for tunneling of the sort considered here are twofold: first, material on either side of the junction must be doped to degeneracy, and secondly, the transition region must be very narrow. To sharpen and give some numerical significance to these terms a very brief review of tunnel diode action will be given here. The theory of tunneling, particularly in germanium, is extremely complex and is still not completely understood, (43, 44, 45) so that our review will be limited to an attempt to obtain a criteria for the impurity profile necessary for noticeable tunneling to occur.

Figure 6 shows the conventional representation for a tunnel diode energy level configuration. The material on both sides is doped to degeneracy; that is, the Fermi level lies within the conduction band on

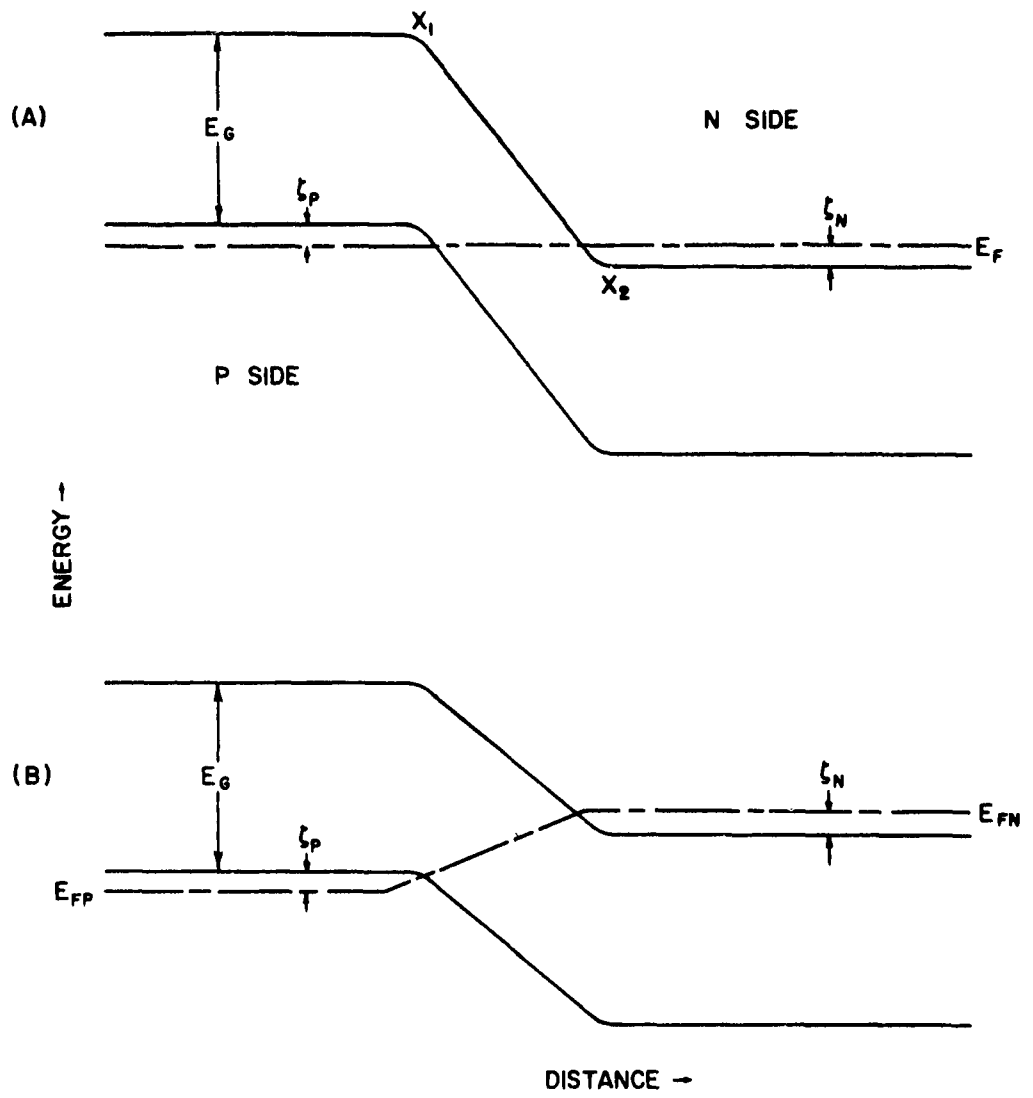

FIGURE 6 TUNNEL DIODE JUNCTION WITHOUT BIAS (A) AND WITH BIAS (B).

the n-side and within the valence band on the p-side. Since with no external voltages applied the Fermi levels on both sides line up, empty states in the valence band sit opposite filled states in the conduction band. When forward bias is applied, the bands uncross until finally there are no longer valence band states opposite conduction band states. It should be noted that we are ignoring band edge smearing and impurity - band effects (46), which become important principally in discussing the valley current.

There is a finite probability that an electron at the band edge of, say, the P-side valence band may cross the so-called forbidden band and enter the N-type conduction band with no loss of energy. At zero bias the density of states function on each side of the junction is such that the flow of tunneling electrons in each direction is equal and no net current flows. With a applied bias, however, the balance is destroyed and there is a net current flow.

The tunneling current density depends on three factors: the distribution of available and filled levels in the coincident bands, the rate at which electrons strike the band edge, and the probability that an electron which strikes the barrier will tunnel through.

The distribution of available and filled levels is found by multiplying the density-of-states function by the Fermi distribution function. The tunneling current due to a particular energy is proportional to the product of the distributions for both sides.

The second factor in the tunneling current is the number of times that the electrons strikes the band edge under the influence of the built-in field in the junction. This picture, as developed by Franz (47) and Spenke (48), pictures the electron as being acted upon by a force $e\vec{\mathcal{E}}$ due to the distortion of the bands. A quasi-classical force-acceleration law is assumed to hold:

$$F = m\frac{dp}{dt} = e\vec{\mathcal{E}} = h\dot{\vec{k}} \quad . \tag{6}$$

The variation in $\vec{k}$ implies a variation in the energy E; each time $\vec{k}$ changes by $\vec{K}$ (a vector in the reciprocal lattice) the energy of the electron goes through all the values of the band. Thus we can consider a frequency of striking the band edge $1/t_o$ as being described by Equation (7)

$$1/t_o = \frac{ae\mathcal{E}}{h} \tag{7}$$

where we have used a simple cubic lattice characterized by a lattice constant a. $\mathcal{E}$ is the field strength in the junction.

The calculation for the tunneling probability has been carried out by several workers (43, 44, 45, 47) and is still the subject of some controversy. We shall use the result of Kane's (43) treatment, which yields as the probability T per incident electron:

$$T \frac{\pi^2}{9} \exp\left[\frac{-\pi m^{*1/2} E_G^{3/2}}{2 \quad 2h\mathcal{E}e}\right] \exp\left[\frac{-B\mathcal{E}}{E_G^{1/2}}\right] \tag{8}$$

where B is a function of k but not of $\mathcal{E}$. If we combine 8, 7, and the distribution term we get a representation for the tunneling current density:

$$J = C_1 \frac{\mathcal{E}}{E_G^{1/2}} \exp\left[\frac{-\pi m^{*1/2} E_G^{3/2}}{2\sqrt{2}\hbar F} \right] \times D(E) \quad . \qquad (9)$$

D(E) represents here the density of state-probability of occupation terms. This term is extremely difficult to evaluate in the case of germanium because of the many-valley characteristic of E(k) for germanium and also because there are two valence bands in germanium. Kane makes an admittedly crude estimate of $\frac{\zeta_n^3 \pi^2 m^* E_G}{12\hbar^2 e^2 \mathcal{E}^2}$ for the value of D at the current peak, with ζ_n being the distance between the Fermi level on the n side and the band edge.

We must now solve for $\mathcal{E}$. If we refer to Figure 6, $\mathcal{E}$ is usually assumed to be the slope of the band edges in the middle of the transition region. The distance W from x_1 to x_2 is found by solving Poisson's equation

$$V''(x) = -\frac{4\pi}{\epsilon} \zeta(x) \qquad (10)$$

where $\zeta(x)$ is the net charge density and ϵ is the dielectric constant. The boundary condition is that the difference in the electrostatic potential on the n-side and on the ζ-side must equal $E_g + \zeta_n + \zeta_p$ this is simply the condition that the Fermi levels on the two sides must be aligned. Simultaneously with (10) it is necessary to satisfy the neutrality condition obtained by equating the number of ionized

impurities to the number of filled conduction band states on the n side and to the number of empty valence band states on the p-side. The solution for the potential distribution is not simple in an arbitrary doping profile, but it has been calculated (43) for the case of an abrupt junction. The result is given in Equation (11):

$$W = \left[\frac{(n+p)\varepsilon V}{2\pi enp} \right]^{1/2} \tag{11}$$

where n and p are the dopant concentrations on the n and p sides, respectively, ε is the dielectric constant, and V is the potential difference between the two sides. If we assume that $n = p = 3 \times 10^{19}$ carriers per c.c. and that $V \approx \Delta E_G \approx 0.7$ e.v., Equation (11) yields a value of W equal to 9.1×10^{-7} cm. Using this, we may calculate the value of ε that appears in Equations (6, 7, 8, and 9). We ignore the curvature in the potential across the junction and assume that any voltage swing necessary to obtain the peak current may be neglected in comparison to E_G. We then write (9) in the form

$$J_{max} = \frac{C_2 W}{(E_G)^{1/2}} \exp \left[\frac{-\pi m^{*1/2} E_G^{1/2} W}{2\sqrt{2}\hbar} \right]. \tag{12}$$

The constant C_2 is difficult to calculate theoretically, due to the complexities of the band structure of germanium. However, capacitance studies (50) tend to indicate the the form of (12) is valid. These measurements also indicate that, for transition regions as thin as we have considered and for doping levels comparable to

those in our example, the current density is on the order of 10^6 amperes/cm^2. Burris, using point-contact diodes and estimating the junction area by microscopically examining the surface after the point had been pulled away, estimated current densities of 10^5 amp/cm^2. The author, using a sectioning technique which will be described later, got values up to 110,000 amperes/cm^2. If we take the highest of these values and assume that it corresponds to the minimum thickness of 9.1×10^{-7} cm, we can obtain the peak tunneling current as a function of W. At W = 200Å., the tunneling current is down to 10^{-4} amps/cm^2, and may be completely ignored. It is obvious that even if we make generous allowances for the crudity of some of the approximations involved, junctions substantially wider than a few hundred angstroms are unlikely to lead to tunneling currents.

Let us now consider the diode equation current and its influence on the i-v, characteristic. The diode equation is

$$J_{Diode} = C_4 (e^{C_{5v}} - 1) \qquad (13)$$

where C_4 and C_5 are constants and V is the applied voltage. Theory predicts (51) that C_4 is a function of mean free paths and diffusion lengths and that C_5 equals e/kT; the former requires data that is difficult to obtain and the latter is only infrequently valid. We shall not discuss the various theories explaining the discrepancies, but shall instead resort to experiment. At this point we should mention the experimental setup used in this study.

Figure 7 shows the jig in which the wire and semiconductor were held during the electrical processing. A spring-loaded micrometer adjustment with an oversize thimble permitted accurately controlled motions with resolution better than 0.0001". One problem which arose with the aluminum wire was that electrolytic pointing or even well-controlled mechanical pointing was impossible, since the rapid rate of oxidation of freshly cut aluminum made it necessary to form the junction almost immediately after snipping. Hence, in some of the diodes formed, the wafer and wire were protected from the atmosphere by a lucite enclosure, so that operation in an inert atmosphere was possible. To expose fresh aluminum a vane of very pure aluminum was touched to the end of the wire and a voltage of about ten volts applied to melt the wire in half, forming a Ball of very clean aluminum on the end (see Figure 8). The vane was then swung out of the way and the wire brought into contact with the wafer.

Figure 9 shows the system in its entirety. A sweep capable of showing the forward and reverse characteristics of devices having peak current levels ranging from 10^{-1} to 10^{-7} amperes was connected to the holder through a mercury switch (to minimize transients due to contact potentials). Also connected through a mercury switch was a pulse supply, timed by the gate pulse from a Tektronix oscilloscope time base generator. The circuit of the pulse amplifier is shown in Figure 10; it consists of a vacuum tube cathode follower driving a transistor inverter, which in turn drives a cascaded

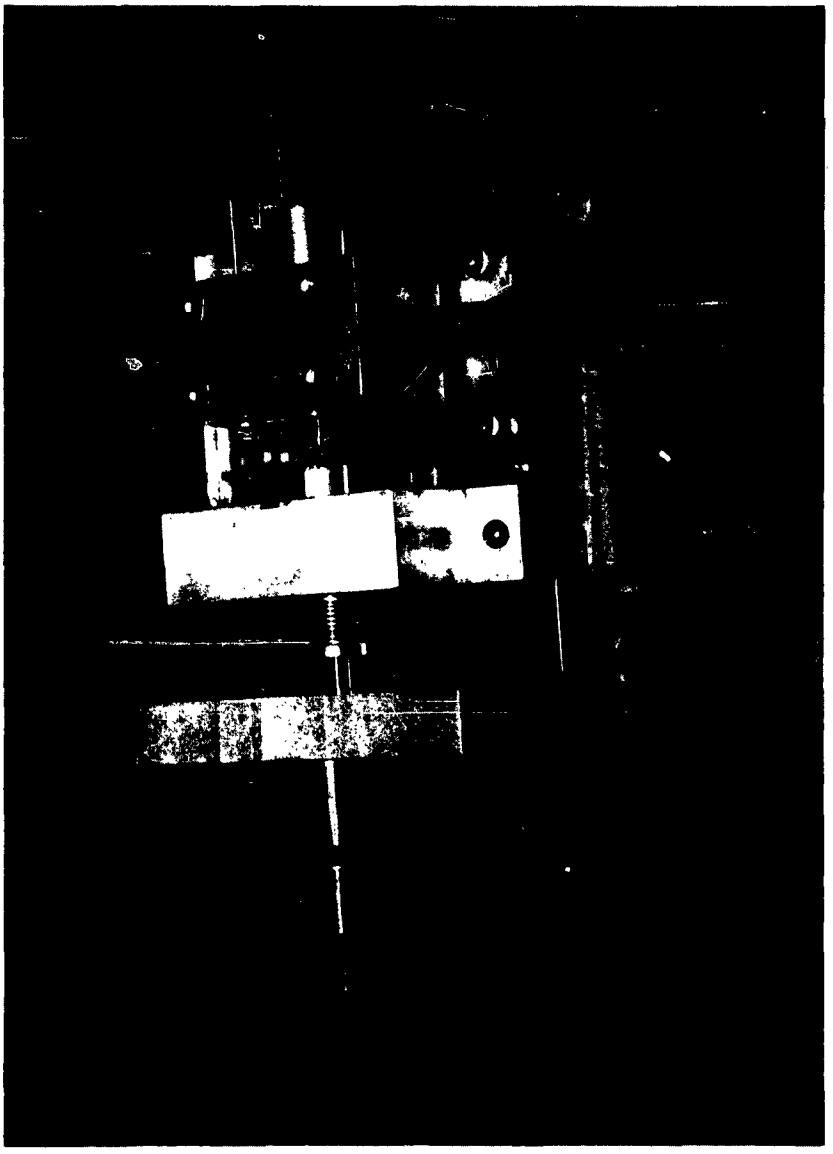

FIGURE 7 DIODE FORMING JIG.

FIGURE 8 ALUMINUM WIRE AFTER FLASHING.

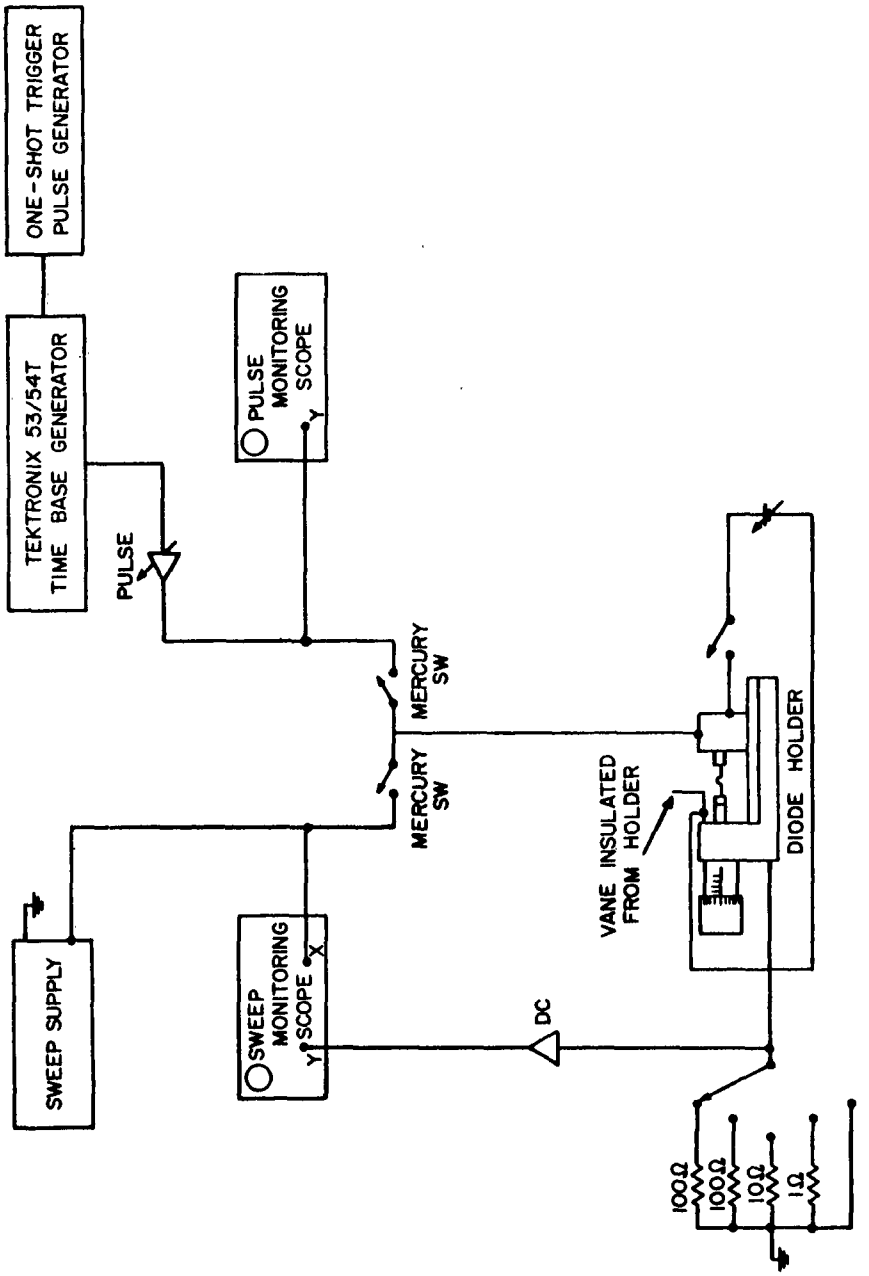

FIGURE 9 FORMING AND MONITORING SYSTEM.

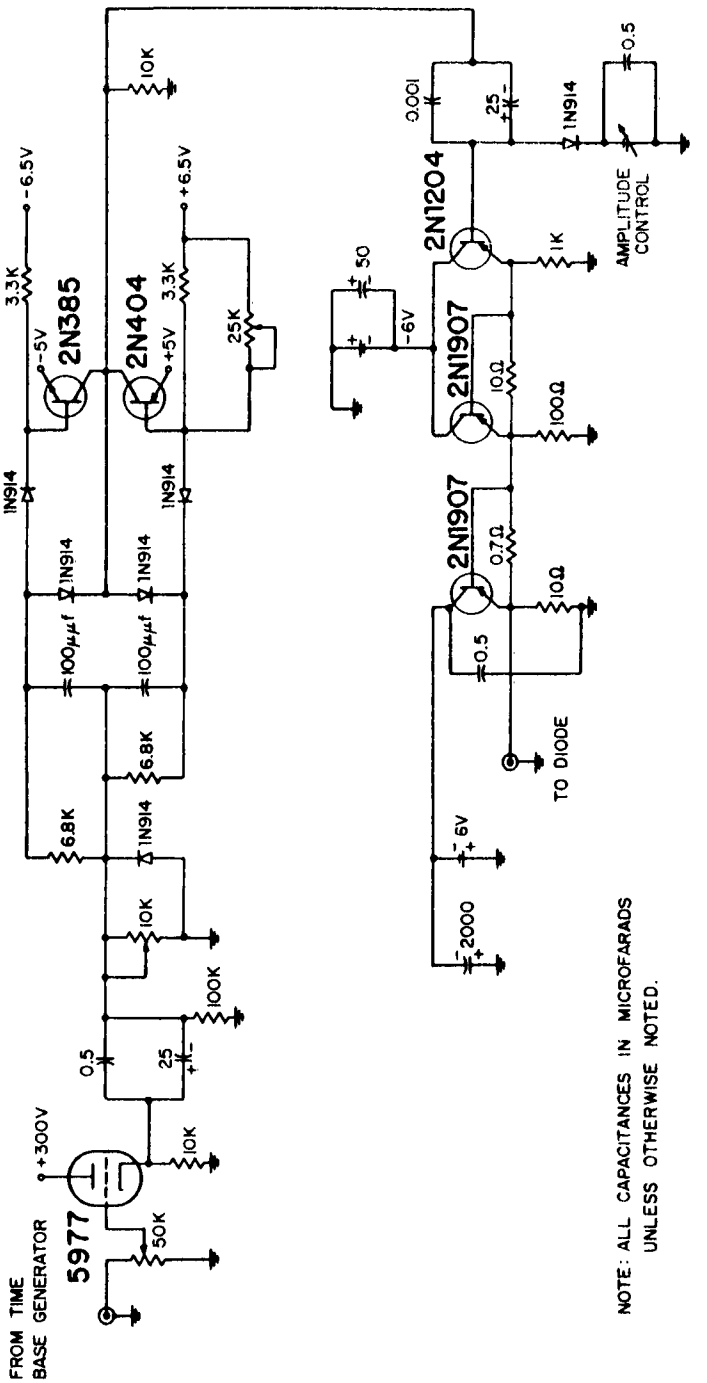

FIGURE 10 PULSE AMPLIFIER.

series of emitter followers. The last two stages were 2N1907 high-frequency diodes in emitter follower configurations with heavy feedback (about 0.7 ohms) between emitter and input. The circuit was capable of putting out pulses of 5-1000 μsec duration and with pulse height variable (by means of a clipper circuit in one of the pre-driver emitter followers) from 0 to 3.8 volts. The rise and fall times were less than 0.5 μsec and the internal impedance was 0.1 ohm. The circuit was capable of putting out 15 ampere pulses at two volts, and was, moreover, capable of tolerating microsecond alterations in the load impedance, which was a somewhat unusual feature of this application.

In measuring the diode characteristic, a freshly snipped or flashed wire was brought down onto the semiconductor until the sweep display at its most sensitive setting indicated current flow. It was then subjected to some particular pulsing format and the picture of its forward and reverse characteristics taken with a scope camera. A split brass form was then carefully clamped in place and epoxy poured around the diode. The potted diode was then carefully ground and polished until the junction was exposed, after which it was examined and photographed with a metallographic microscope. A typical section is shown in Figure 11. The technique is hampered by the variation in hardness between the germanium, the aluminum wire, and the epoxy; abrasives suitable for giving a good reflective finish to germanium tend to scoop and undercut the aluminum and the germanium epoxy interface.

FIGURE 11 CROSS-SECTION OF POINT-CONTACT DIODE.

Moreover, the welded point tends to set up a stressed condition in the germanium in the immediate neighborhood of the point which the grinding appears to aggravate, with the result that chipping and "cribbing" often results. However, usable data was obtained. Some measurements were also made by pulling the wire off and examining the spot where it had been (Figure 12). This is for a relatively high current unit. Note that there appears to be a relatively symmetrical shear area, probably coinciding with faults introduced during forming. The rough region presumably corresponds to the P-N junction area.

Part of the results are shown in Figure 13. Diodes 3-24, 3-25, are 3-26 were formed by pulsing with relatively high-impedance (100 ohm) sources; if we refer to Equation (13), these have a value of C_5 equal to 7.25. Diodes 3-27, 3-28, and 3-27 were formed by pulsing with a low-impedance (0.1 ohm) supply; these yielded a value of C_5 equal to 15.75. The reason for the variation of C_5 in diodes is rather poorly understood (3).

Now let us use some of our experimental results to estimate the degree of importance of junction effects. The incremental conductance of a diode may be found by differentiating Equation (13):

$$\sigma_D = \pi a^2 C_4 C_5 e^{C_5 V} \qquad (14)$$

where a is the radius of the contact. The spreading conductance is (3)

$$\sigma_s = \frac{4a}{\rho} \qquad (15)$$

FIGURE 12 VERTICAL VIEW OF JUNCTION AFTER WIRE IS REMOVED.

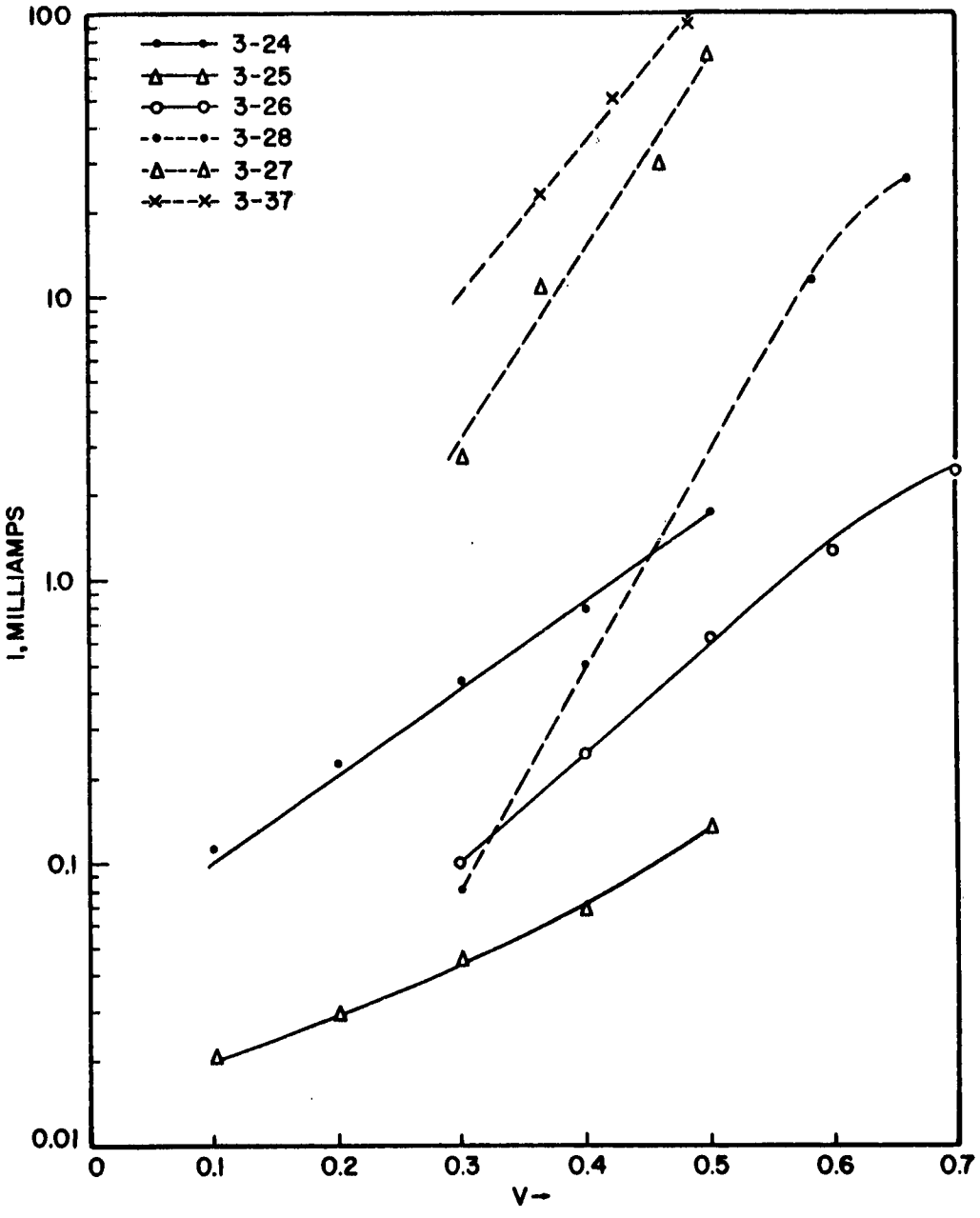

FIGURE 13 DIODE CHARACTERISTICS.

where ρ is the resistivity of the material. The forward voltage at which the spreading resistance comes into play may be found by setting (14) equal to (15) and solving for x:

$$V = \frac{1}{C_5(0.4343)} \log_{10} \left[\frac{4}{\pi a \rho C_4 C_5} \right]$$

The largest value of a encountered in our work was $a = 10^{-3}$ cm, and the material was 10^{-3} ohm-cm. An average value of C_4 obtained by microscopic examinations of the type described earlier was 10^4 amps/cm^2. This leads to a value of V equal to 0.568 volts. Figure 13 shows the I-V characteristic at high current levels for a diode for which $a = 10^{-3}$ cm. Note the sudden break between 0.5 and 0.6 volts, corresponding to this transition. The maximum voltage at which junction effects are important is $V = E_g + \zeta_n + \zeta_p$, since at higher forward bias the junction has effectively disappeared. This will be around 0.7 volts for germanium. Hence we may expect that junction effects may be taken into account by postulating a series voltage source of between 0.57 and 0.7 volts, depending upon the area of the contact.

Little success was obtained in forming using reverse pulses, and the reverse characteristics varied too widely to permit characterization in any simple and practical manner . Close empirical fit was often possible to the Zener-like expression in (18):

$$I_{Rev} = C_6(V - C_7)^2 \quad . \tag{18}$$

The variation of C_6 and C_7 was too gross to allow a very useful generalization to be made; roughly, junction effects appeared to dominate spreading resistance out to about 1 volt.

IV. COMPUTATION OF CRITICAL BREAKDOWN VOLTAGE

When a metal point is applied to a semiconductor and a voltage applied across the combination, the flow of current through the resistive bulk semiconductor material will generate a certain amount of heat, giving rise to a temperature gradient within the material. Intuition indicates and more rigorous analysis proves that the highest temperature will be associated with the material immediately adjacent to the point. If the applied voltage is high enough, either the wire or the semiconductor will melt in the vicinity of the interface. From the point of view of forming studies, the voltage at which this occurs is a critical one, and it is the purpose of this section to solve for it and to check the analytical results by experiment.

Torrey and Whitmer (3) attacked this problem for the case in which the thermal and electrical resistances are constant with temperature, and Sim solved it assuming the electrical conductivity to vary with temperature and the thermal conductivity to be constant with temperature. Following the treatment in Section II, we shall assume that the electrical conductivity is constant while the thermal conductivity varies in the manner shown in Figure 3.

Figure 14 shows the metal-semiconductor contact. We assume that $\sigma_m >> \sigma_s$, so that the interface will be an equipotential plane. Also, if the metal is molten at the interface, we may assume

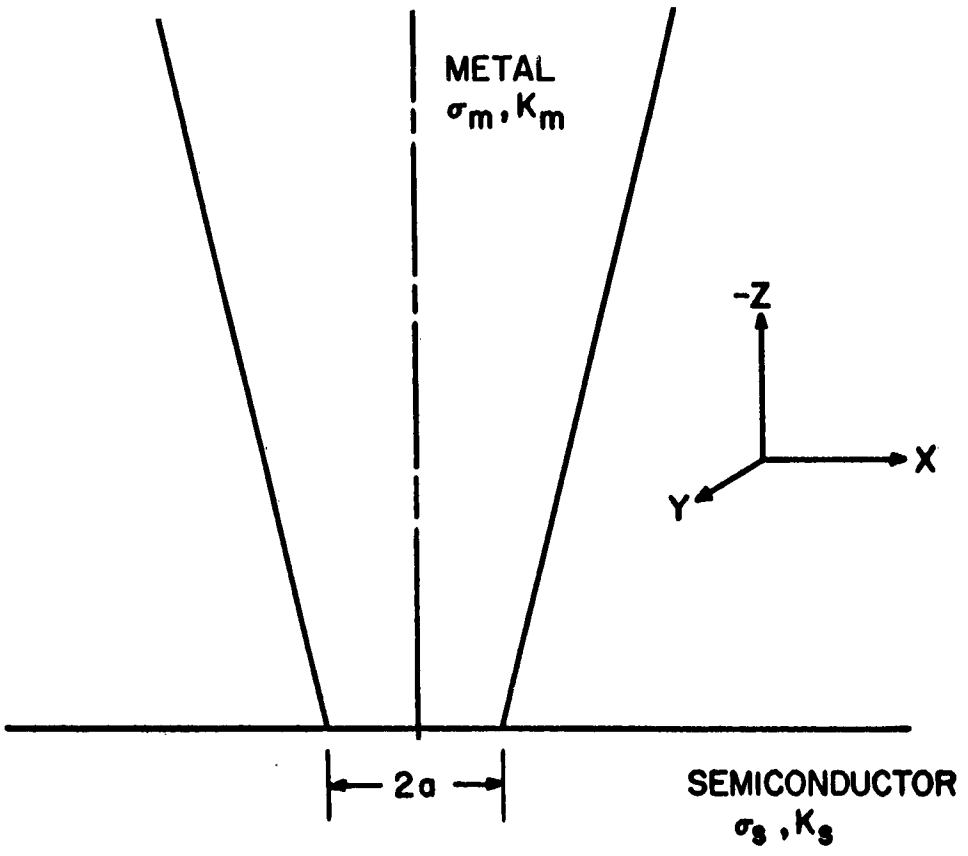

FIGURE 14 THE METAL-SEMICONDUCTOR CONTACT.

that the metal-semiconductor interface is an isotherm at the melting point of the contact material. It is obvious also that there is going to be a high degree of cylindrical symmetry to the problem. The form best suited to expressing these conditions is the oblate spheroidal coordinate system. (Figure 15)

In this system, the orthogonal surfaces may be written in the forms shown in Equations (18)and(19).

$$\frac{z^2}{a^2\zeta^2} + \frac{\rho^2}{a^2(1+\zeta^2)} = 1 \tag{18}$$

$$\frac{\rho^2}{a^2(1-\xi)^2} - \frac{z^2}{a^2\xi^2} = 1 \tag{19}$$

where

$$\rho^2 = x^2 + y^2 \tag{20}$$

In addition, there are planes of constant azimuthal angle ϕ.

The matrics are

$$h_\xi = a\left[\frac{\xi^2+\zeta^2}{1-\xi^2}\right]^{1/2} \qquad h_\zeta = a\left[\frac{\xi^2+\zeta^2}{1+\zeta^2}\right]^{1/2} \tag{21}$$

$$h_\phi = a\left[(1+\zeta^2)(1-\xi^2)\right]^{1/2}$$

In a conducting medium with negligible charge accumulation, $\nabla \cdot \vec{J} = 0$, where $\vec{J}$ = the current density. Thus,

$$\vec{J} = -\sigma_s \nabla V \tag{22}$$

so

$$\nabla \cdot (-\sigma_s \nabla V) = 0 \quad . \tag{23}$$

We now make use of the assumption of constant electrical conductivity which we developed in Section II. This permits us to take the σ_s term in (23) over to the left of the gradient operator, giving us LaPlaces' equation:

$$-\sigma \nabla^2 V = 0 \tag{24}$$

or, in our particular coordinate system:

$$\frac{\partial}{\partial \xi}\left[(1-\xi^2)\frac{\partial V}{\partial \xi}\right] + \frac{\partial}{\partial \zeta}\left[(1+\zeta^2)\frac{\partial V}{\partial \zeta}\right] + \frac{^2+\zeta^2}{(1+\zeta^2)(1-\ ^2)}\frac{\partial^2 V}{2\phi^2} = 0 \tag{25}$$

$\partial/\partial \phi = 0$ from symmetry, so that (25) becomes:

$$\frac{\partial}{\partial \xi}\left[(1-\xi^2)\frac{\partial V}{\partial \xi}\right] + \frac{\partial}{\partial \zeta}\left[(1+\zeta^2)\frac{\partial V}{\partial \zeta}\right] = 0 \quad . \tag{26}$$

Assume:

$$V = A(\xi)\, B(\zeta) \quad . \tag{27}$$

This permits us to separate the equation

$$\frac{d}{d\xi}\left[(1-\xi^2)\frac{dA}{d\xi}\right] + n(n+1)\, A = 0 \tag{28}$$

$$\frac{d}{d\zeta}\left[(1+\zeta^2)\frac{dB}{d\zeta}\right] - n(n+1)\, B = 0 \quad . \tag{29}$$

We shall assume that the electrical conductivity of the point material is so much higher than that of the semiconductor that the metal-semiconductor interface is an equipotential. Hence $\frac{dA}{d\xi}$ must vanish and so must n. Then (29) becomes

$$\frac{d}{d\zeta}\left[(1+\zeta^2)\frac{dB}{d\zeta}\right] = 0 \qquad (30)$$

solving for B,

$$B = C\tan^{-1}\zeta + D = V(\zeta) \qquad . \qquad (31)$$

To solve for C and D we set the potential V equal to zero at $\zeta = -\infty$ and equal to V_o, the effective applied voltage, at $\zeta = 0$. Then:

$$V = V_o\left[1 - \frac{2}{\pi}\tan^{-1}\zeta\right] \qquad . \qquad (32)$$

Let P equal the power input per unit volume due to ohmic power loss. Then:

$$P = \sigma_s(\nabla V^2) = \sigma_s\left[\frac{1}{h_\zeta}\frac{\partial V}{\partial \zeta}\right]^2 = \frac{4V_o^2\sigma_s}{\pi^2 a^2(\xi^2+\zeta^2)(1+\zeta^2)} \qquad . \qquad (33)$$

This is the same as the Torrey-Whitmer result for power distribution. We shall now solve for the temperature distribution. We can write the heat flow equation, setting the heat flux out of the material equal to the ohmic power input.

$$\nabla \cdot K\nabla T - \frac{4V_o^2}{\pi^2 a^2(\xi^2+\zeta^2)(1+\zeta^2)} = 0 \qquad . \qquad (34)$$

We have already assumed that the metal-semiconductor junction is an equipotential surface; we may also see that it is an isothermal surface, at a temperature equal to the fusion temperature

of the point material. It has been shown (1) that, with configurations of this sort, if the equipotential and isothermal surfaces coincide at one surface, they coincide throughout. Hence we are justified in setting

$$\frac{\partial T}{\partial \phi} = \frac{\partial T}{\partial \xi} = 0 \quad . \tag{35}$$

This reduces Equation (34) to:

$$\frac{1}{h_\xi h_\phi h_\zeta} \frac{d}{d\zeta}\left[K \frac{h_\xi h_\phi}{h_\zeta} \frac{dT}{d\zeta}\right] = \frac{4V_o^2\sigma_s}{\pi^2 a^2} \frac{1}{(\xi^2+\zeta^2)(1+\zeta^2)} \tag{36}$$

which reduces to

$$\frac{d}{d\zeta}\left[K(1+\zeta^2)\frac{dT}{d\zeta}\right] = \frac{4V_o^2\sigma_s}{\pi^2(1+\zeta^2)} \quad . \tag{37}$$

Integrating once,

$$K(1+\zeta^2)\frac{dT}{d\zeta} = \frac{4V_o^2\sigma_s \cos^{-1}\zeta}{\pi^2} \tag{38}$$

or

$$\frac{dT}{d\zeta} = -\frac{4V_o^2\sigma_s}{\pi^2 K} \cdot \frac{\cot^{-1}\zeta}{1+\zeta^2} \quad . \tag{39}$$

We cannot integrate this exactly, because of the irregular variation of K with T and hence with ζ. However, its numerical solution poses no particular problem; this has been carried out and the results plotted in Figure 16.

We shall now simultaneously check Figure 16 and the conclusions of Section III by a simple experiment. To do this we find the melting temperature of the point material (or of germanium if it is the less refractory) and use Figure 16 to find the effective

voltage. To this must be added the series voltage due to junction effects, as calculated in the preceeding section.

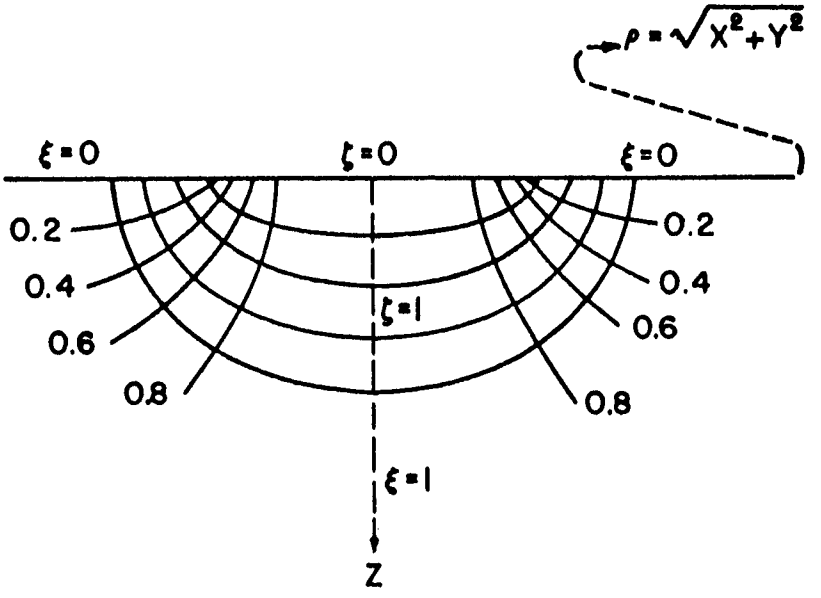

FIGURE 15 THE OBLATE SPHEROIDAL COORDINATE SYSTEM.

In our case the point material melts before the semiconductor, at a temperature which we may estimate from the aluminum-boron phase diagram (53) as being approximately 920° K. Referring to the chart of Figure 16, this corresponds to an effective applied voltage of 0.62 V necessary to cause breakdown. The diode used in Section III as an example was also used here. Referring back to the calculation of Section III, we see that the effective series voltage due to junction effects is 0.57

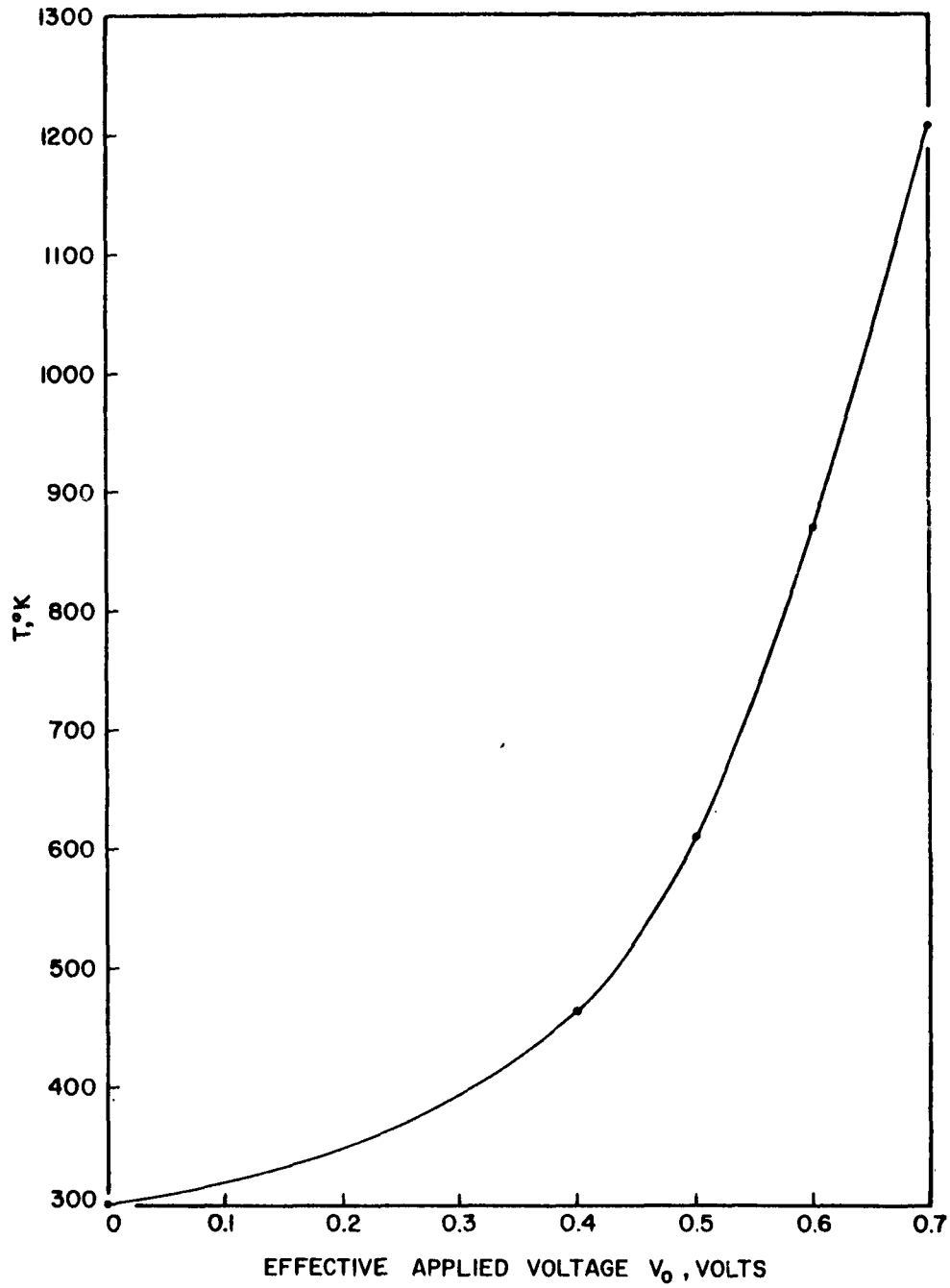

FIGURE 16: VARIATION OF TEMPERATURE AT INTERFACE WITH EFFECTIVE APPLIED VOLTAGE.

volts. Thus the applied voltage necessary for breakdown should be 0.62 volts plus 0.57 volts, a total of 1.19 volts.

To measure the breakdown we apply sweep voltage of increasingly higher amplitude to the diode, from a moderately high-impedance supply. After each time that the diode is subjected to a sweep voltage of particular peak amplitude, the circuit is switched to a more sensitive setting and the current at a forward bias of 0.1 volt measured. As we shall see later, the thermal time constant of the diode configuration is on the order of microseconds, so that the fact that we are using a 60-cycle sweep rather than dc will have no effect. The results of the measurement are shown in Figure 17. The reason for the slight descending characteristic at the lower values of sweep voltage is not known. However, it is clear that a sharp breakdown, presumably due to a melting of the point, took place at 1.17 volts. This represents an error of less than 2 per cent in our original estimate of 1.19 volts. The reason that the current after breakdown was not higher was that, as soon as the diode began breaking down and more current flowed, the sweep voltage dropped due to the series impedance of the pulse supply. Thus it was not necessary to take into account the effects of exceeding the critical voltage, a subject which will be considered in the next section.

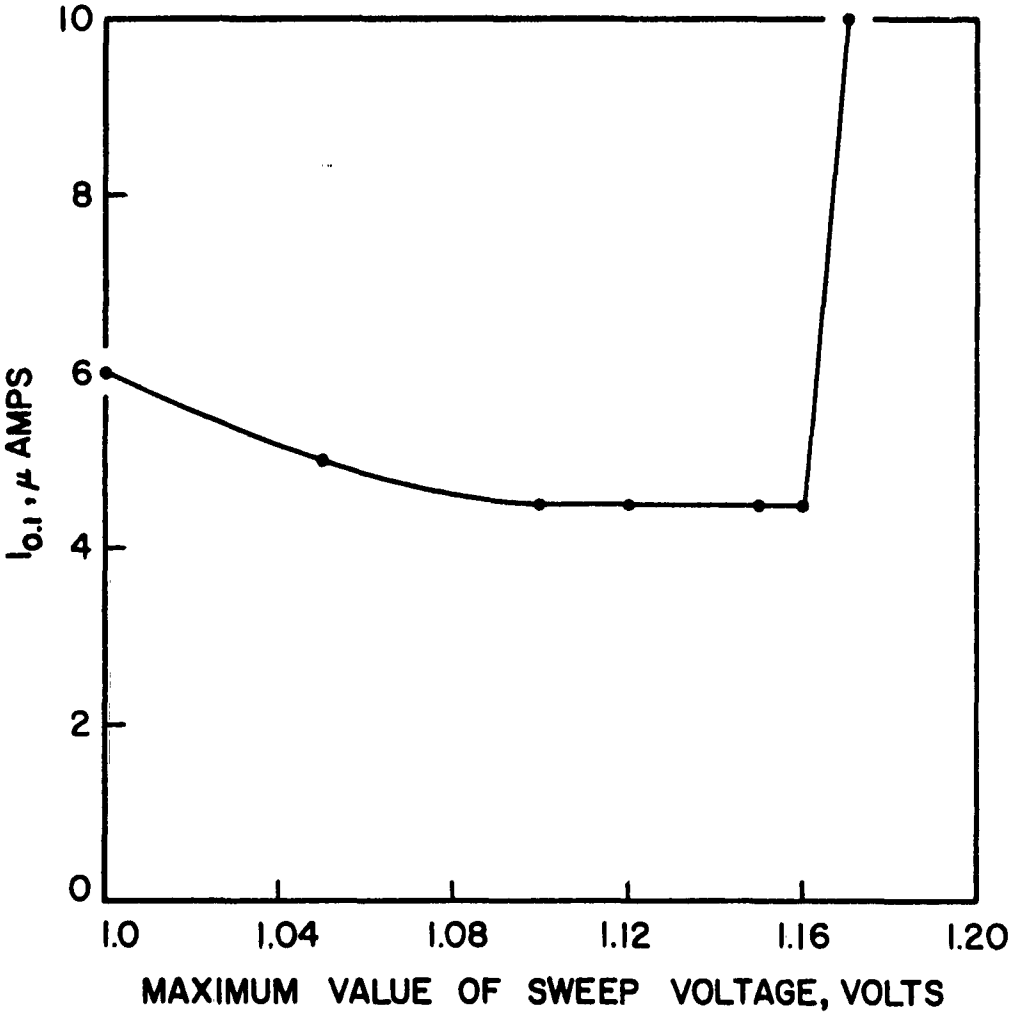

FIGURE 17: $I_{0.1}$ VERSUS MAXIMUM FORWARD SWEEP VOLTAGE.

V. THE THERMAL PROFILE AND DIODE CONFIGURATION FOR VOLTAGES HIGHER THAN CRITICAL

We saw in the previous section that, as the voltage applied to a lightly formed diode was increased, a value of voltage was finally reached at which melting of the point began. We shall now analyse the case where the voltage is higher than this critical value.

Figure 18 shows a diode being subjected to heavy forming. The heating causes the formation of a molten eutectic mixture of point material and semiconductor, the solid germanium having been partially melted out in a crater beneath the point.

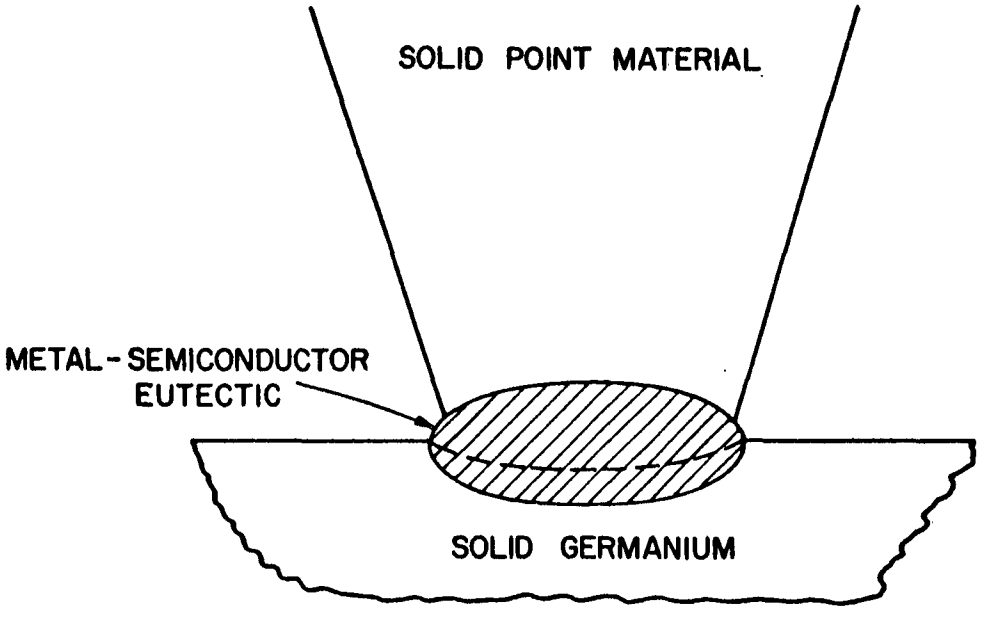

FIGURE 18 DIODE SUBJECTED TO HEAVY FORMING.

It is quite difficult to make any very intelligent guesses about the conductivity of the molten eutectic, there being relatively little data available on metal-semiconductor alloys. As crude approximation, we shall assume it to be equal to that of the pure semiconductor. This will permit us to use the simplified potential distribution analysis of Section IV.

It would also be interesting to simultaneously investigate the possibility that thermoelectric effects play a part in the forming process (54, 55).

The three most important thermoelectric effects not involving magnetic fields are the Seebeck effect, the Thompson effect, and the Peltier effect. They are so closely related that the simplest way to understand any one of them is to consider all three.

When a circuit composed of two dissimilar materials is such that one junction is at a different temperature than the other, (see Figure 19) there will be developed, in general, an E.M.F. U_{12}. The thermoelectric power α_{12} is then defined by Equation 40.

$$\alpha_{12} = \lim_{\Delta T \to 0} \frac{U_{12}}{\Delta T} \quad . \qquad (40)$$

ΔT is the temperature difference between the two junctions. We shall discuss the sign convention later.

The Peltier effect may be thought of as the converse of the Seebeck effect. When current is passed across the junction between

two dissimilar metals, the junction absorbs or liberates a quantity Q_{12} of heat per unit area, proportional to the current density J.

$$-Q_{12} = \pi_{2,1} J = Q_{21} \quad . \qquad (41)$$

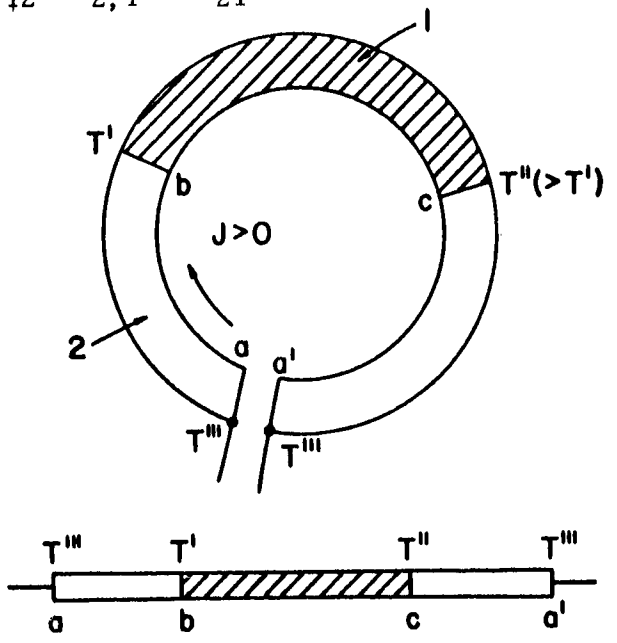

FIGURE 19 THERMOELECTRIC EFFECTS.

In contrast to the Peltier and Seebeck effects,the Thompson effect relates to a single material rather than to contacting materials. The Thompson effect relates to the reversable absorption or liberation of heat which occurs when a current flows along a thermal gradient. Equation 42 defines the Thompson coefficient T in terms of the thermal gradient $\frac{dT}{dx}$, the current density J and the heat per unit volume Q_{th} generated.

$$Q_{th} = T\ J \frac{dT}{dx} \quad . \qquad (42)$$

At this point, a word regarding signs is in order. Suppose in Equation (40) that ΔT is always taken as positive. Then U_{12} is considered positive if, in an open bimetal circuit such as that shown in Figure 19, the terminal connected to the high temperature side is positive. Still referring to Figure 19, $Q_{1,2}$ is the heat withdrawn from the environment at terminal a, while Q_{21} is the heat withdrawn from the environment at terminal b. Thus, if terminal b heats up, then Q_{21} is a negative number; if it cools down, Q_{21} is a positive number. In Equation (42), if T is positive and if the conventional flow of current is in the direction of increasing temperature, then heat is absorbed from the environment.

The three thermoelectric coefficients are linked by Equations (43) and (44), commonly known as the Thompson relations:

$$\alpha_{12} = \frac{\pi_{12}}{T} \qquad (43)$$

$$\frac{d\alpha_{1,2}}{dT} = \frac{\tau_2 - \tau_1}{T} \quad . \qquad (44)$$

Although these relations were originally developed using classical concepts, they have been proven valid by quantum mechanical treatments also.

Equation (44) permits us to divide $\alpha_{1,2}$ into two portions, each of which is dependent upon one material:

$$\alpha_{1,2} = \alpha_2 - \alpha_1 \tag{45}$$

where

$$\alpha_1 = \int_0^T \frac{\tau_1}{T}\, dT \tag{46}$$

and

$$\frac{\tau_1}{T} = \frac{d\alpha_1}{dT} \tag{47}$$

It thus becomes meaningful to speak of the thermoelectric power of a single material. Experimentally this is a great help, since it is often much easier to measure thermoelectric power than to measure the Thompson coefficient directly.

Unfortunately for our purposes, neither theoretical nor experimental work has been done on the thermoelectric parameters of germanium as heavily doped as that which we are using. Johnson and Lark-Horowitz (56) considered the case where the doping was sufficient that ionized impurity scattering was the dominant obstacle to carrier motion; however, they did not consider degenerate material and employed Boltzmann Statistics. Their results, together with the experimental results of Middleton and Scanlon (57), are shown in Figure 20. The knees of the curves occur at temperatures where intrinsic conduction becomes important. We have seen that in our case this happens only at temperatures approaching the melting point of germanium.

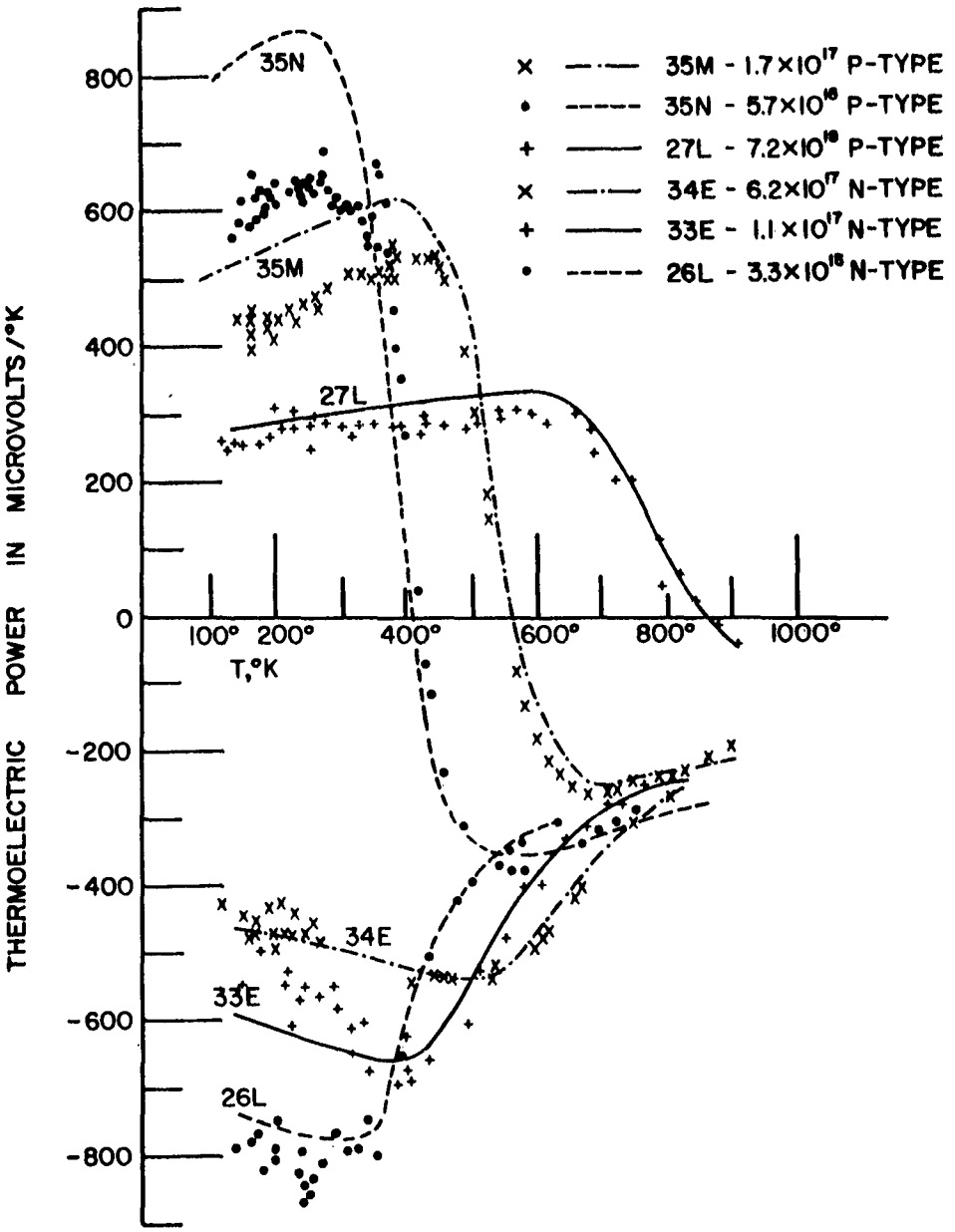

FIGURE 20 THERMOELECTRIC POWER IN GERMANIUM (AFTER JOHNSON AND LARK-HOROVITZ).

Johnson[55] derives an expression for the Thompson coefficient valid for semiconductors at all doping levels.

$$\tau = \frac{\partial}{\partial T}\left(\frac{A_{21}}{A_{11}}\right) + \frac{A_{12}}{A_{11}} \tag{47}$$

where

$$A_{11} = \frac{-8\pi e^2}{3(m^*)^2}\int_o^\infty \ell\varepsilon \frac{\partial f_o}{\partial \varepsilon}\, d\varepsilon \tag{48}$$

$$A_{12} = \frac{8\pi e}{3(m^*)^2}\int_o^\infty \varepsilon\ell \frac{\partial f_o}{\partial \varepsilon}\left[\frac{\varepsilon}{T} + T\frac{d}{dT}\left(\frac{\zeta}{T}\right)\right] d\varepsilon \tag{49}$$

$$A_{21} = \frac{8\pi e}{3(m^*)^2}\int_o^\infty \varepsilon^2\ell \frac{\partial f_o}{\partial \varepsilon}\, d\varepsilon \tag{50}$$

and, combining these with (46),

$$\alpha = -\frac{1}{eT}\frac{\int_o^\infty \varepsilon^2\ell(\partial f_o/\partial\varepsilon)d\varepsilon}{\int_o^\infty \varepsilon\ell(\partial f_o/\partial\varepsilon)\, d\varepsilon} + \frac{\zeta}{eT} \quad . \tag{51}$$

e is the charge on the electron, ε is the energy, measured from the bottom of the valence band, $f_o(\varepsilon)$ is the unperturbed energy distribution function, ℓ is the mean free path, ζ is the Fermi level, and m^* is the electron effective mass.

It might be noted that A_{11} is the conductivity of the material. One is tempted to use the results of Section II and assume it constant; however, we must bear in mind that, in Section II, we were only interested in the variation in resistivity compared to the average resistivity, while here we are interested in the derivative.

It is now necessary to obtain some of the terms occurring in Equations (48, 49, and 50). The variation of ζ with temperature in heavily doped germanium was studied by Blakemore (58); his results are shown in Figure 21. Note that the energy gap between the bottom of the conduction band and the top of the valence band narrows with increasing temperature.

In order to write the f_o term, it is first necessary to know $N(\epsilon)$. An expression which takes rough account of the effect of the many-valley E(k) characteristic and of the anisotropic energy surfaces is given in Equation (52).

$$N(\epsilon) = \frac{16\pi}{h^3}\left[2m_{\|}\, m_{\perp}^2\right]^{1/2} \epsilon^{1/2} = 3.51 \times 10^{29}\, \epsilon^{1/2} \tag{52}$$

where $m_{\|}$ and $m_{\perp}$ are effective masses relating to the curvature of the band along two different directions.

The mean free path ℓ may be calculated by means of the Conwell-Weisskopf formula (36).

$$\ell = \frac{k^2 \epsilon_o^2 \epsilon^2}{\pi N e^4 \ell n\left[1+k^2 \epsilon_o^2 d^2 e^{-4}\right]} \tag{53}$$

where k is the dielectric constant of germanium, ϵ_o is the permittivity of free space, ϵ is energy, N is the dopant density, d is the average distance between impurities, and e is the electronic charge. The calculation was carried out and the results are shown in Figure 22.

It is now necessary to obtain some of the terms occurring in Equations (48, 49, and 50). The variation of ζ with temperature in heavily doped germanium was studied by Blakemore (58); his results are shown in Figure 21. Note that the energy gap between the bottom of the conduction band and the top of the valence band narrows with increasing temperature.

In order to write the f_o term, it is first necessary to know $N(\epsilon)$. An expression which takes rough account of the effect of the many-valley E(k) characteristic and of the anisotropic energy surfaces is given in Equation (52).

$$N(\epsilon) = \frac{16\pi}{h^3}\left[2m_{\parallel} m_{\perp}^2\right]^{1/2} \epsilon^{1/2} = 3.51 \times 10^{29}\, \epsilon^{1/2} \tag{52}$$

where $m_{\parallel}$ and $m_{\perp}$ are effective masses relating to the curvature of the band along two different directions.

The mean free path ℓ may be calculated by means of the Conwell-Weisskopf formula (36).

$$\ell = \frac{k^2 \epsilon_o^2 \epsilon^2}{\pi N e^4 \ell n\left[1+k^2 \epsilon_o^2 d^2 e^{-4}\right]} \tag{53}$$

where k is the dielectric constant of germanium, ϵ_o is the permittivity of free space, ϵ is energy, N is the dopant density, d is the average distance between impurities, and e is the electronic charge. The calculation was carried out and the results are shown in Figure 22.

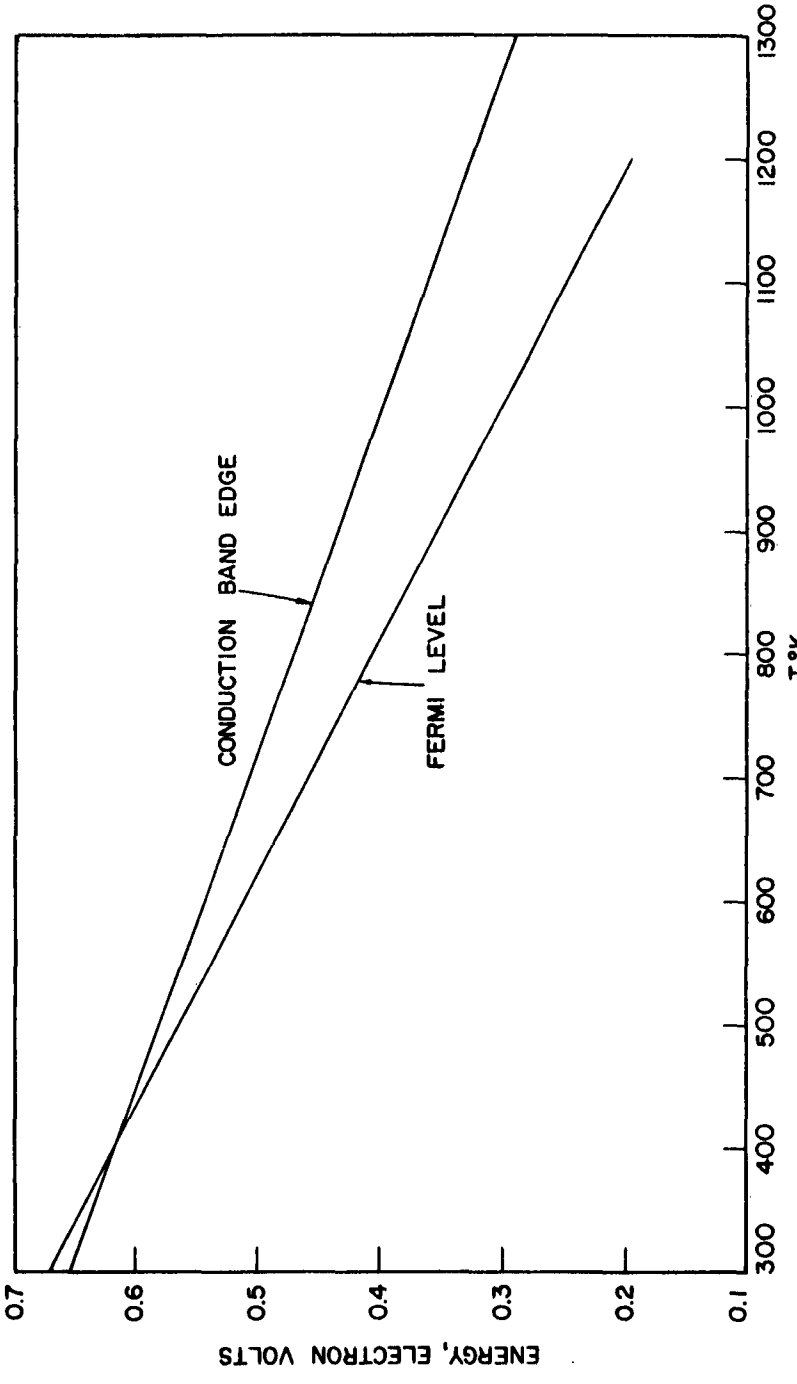

FIGURE 21 VARIATION OF FERMI LEVEL WITH TEMPERATURE $N_D = 3 \times 10^{19} \frac{\text{atoms}}{\text{cc}}$.

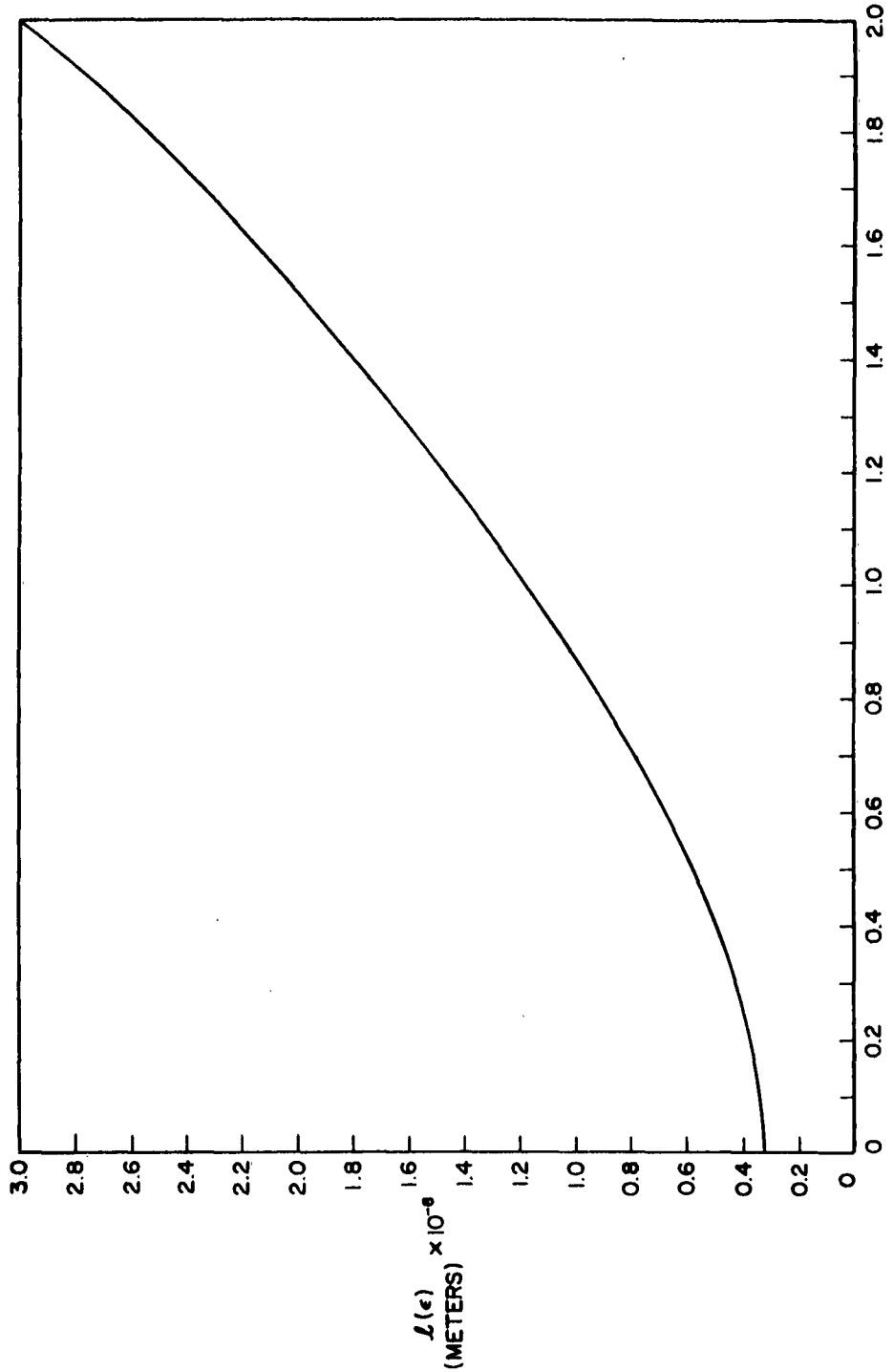

FIGURE 22 MEAN FREE PATH VERSUS ELECTRON ENERGY $N_D = 3 \times 10^{19} \frac{\text{atoms}}{\text{cc}}$.

We can combine (52) with the Fermi-Dirac distribution function to obtain $f_o(\epsilon)$

$$f_o(\epsilon) = \frac{3.51 \times 10^{29} \epsilon^{1/2}}{1 + \exp\left[\frac{\epsilon - \zeta}{kT}\right]} \tag{54}$$

combining this with (51) and simplifying,

$$\alpha = \frac{1}{T}\left\{\zeta - \frac{\int_o^\infty \left[\frac{\ell \epsilon^{3/2}}{2\left(1+\exp\left[\frac{\epsilon-\zeta}{kT}\right]\right)} - \frac{\ell \epsilon^{5/2} \exp\left[\frac{\epsilon-\zeta}{kT}\right]}{kT\left(1+\exp\left[\frac{\epsilon-\zeta}{kT}\right]\right)^2}\right] d\epsilon}{\int_o^\infty \left[\frac{\ell \epsilon^{1/2}}{2\left(1+\exp\left[\frac{\epsilon-\zeta}{kT}\right]\right)} - \frac{\ell \epsilon^{3/2} \exp\left[\frac{\epsilon-\zeta}{kT}\right]}{kT\left(1+\exp\left[\frac{\epsilon-\zeta}{kT}\right]\right)}\right] d\epsilon}\right\} . \tag{55}$$

This was calculated using the values of ζ from Figure 21 and of ℓ from Figure 22. The results are shown in Figure 23; they appear to be a reasonable extension of the data in Figure 20.

The slope of the thermoelectric power curve, multiplied by T, is the Thompson coefficient. To a good approximation the curvature of $\alpha(T)$ may be neglected, and we may write:

$$\zeta = -0.16 \text{ T microvolts}/^{\circ}\text{K} \tag{56}$$

for germanium of this doping level.

We shall now generalize Equation (42) to a three-dimensional case and add the heat source so obtained to the I^2R heat source in Equation (34).

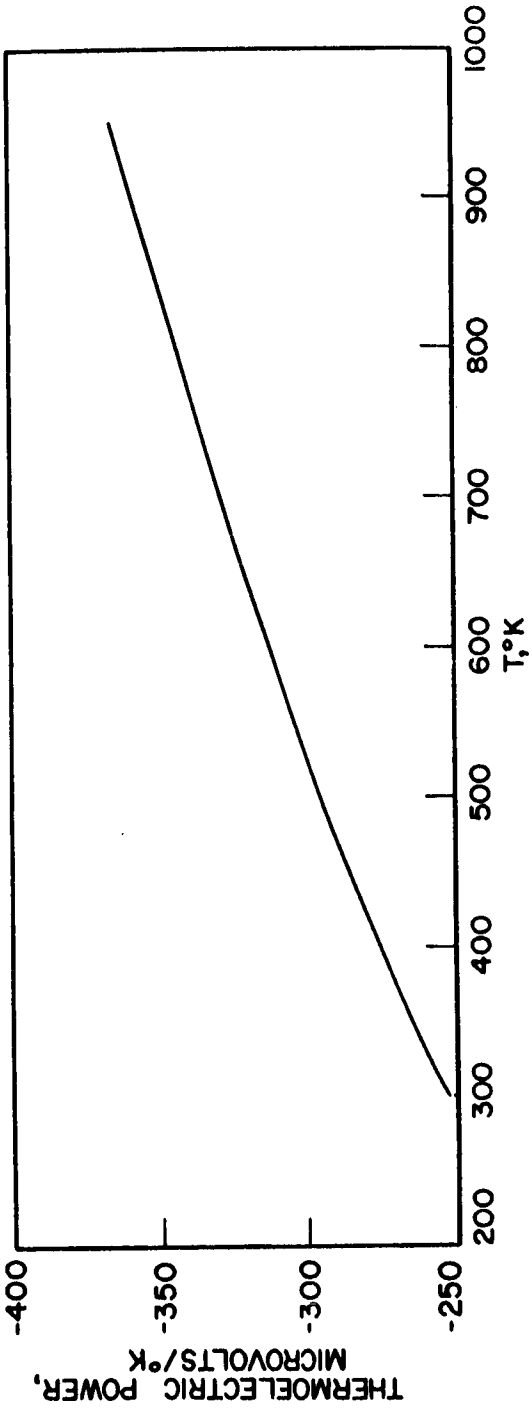

FIGURE 23 THERMOELECTRIC POWER FOR GERMANIUM. $N_D = 3 \times 10^{19} \frac{\text{carriers}}{\text{cc}}$.

$$\nabla \cdot (k \nabla T) - \frac{4V_o^2 \sigma_s}{\pi^2 a^2 (\xi^2+\zeta)(1+\zeta^2)} + \tau \vec{J} \cdot \nabla T = 0 \quad . \qquad (57)$$

The current density may be derived from the expressions of Section IV.

$$\vec{J} = - \sigma_s \nabla V = \frac{2V_o \sigma_s}{\pi a \sqrt{(\xi^2+\zeta^2)(1+\zeta^2)}} \qquad (58)$$

Next we express $\nabla \cdot (k \nabla T)$ in terms of $\xi \zeta \phi$ coordinates:

$$\nabla \cdot (k \nabla T) = \frac{1}{h_\xi h_\phi h_\zeta} \frac{d}{d\zeta} \left[k \frac{h_\xi h_\phi}{h_\zeta} \frac{dT}{d\zeta} \right] = \frac{1}{a^2(\xi^2+\zeta^2)} \frac{d}{d\zeta} \left[k(1+\zeta^2) \frac{dT}{d\zeta} \right] \qquad (59)$$

and finally, writing out the third term in (57)

$$\tau J \cdot \nabla T = \left(\frac{2V_o \sigma_s \tau}{\pi a (\xi^2+\zeta^2)(1+\zeta^2)} \right) \cdot \frac{1}{h_\zeta} \frac{\partial T}{\partial \zeta} = \frac{2V_o \sigma_s \tau}{\pi a^2 (1+\zeta^2)} \frac{\partial T}{\partial \zeta} \quad . \qquad (60)$$

We shall evaluate the temperature profile along the centerline ($\xi = 1$). Then (57) becomes

$$\frac{1}{a^2(1+\zeta^2)} \frac{d}{d\zeta} \left[k(1+\zeta^2) \frac{dT}{d\zeta} \right] - \left[\frac{2V_o}{\pi a (1+\zeta^2)} \right]^2 \sigma_s + \frac{2V_o \sigma_s \tau}{\pi a^2 (1+\zeta^2)} \frac{\partial T}{\partial \zeta} = 0 \qquad (61)$$

simplifying,

$$\frac{d}{d\zeta} \left[k(1+\zeta^2) \frac{dT}{d\zeta} \right] - \frac{4V_o^2 \sigma_s}{\pi^2 (1+\zeta^2)} + \frac{2V_o \sigma_s \tau}{\pi} \frac{dT}{d\zeta} = 0 \quad . \qquad (62)$$

This was solved by numerical computation for $V_o = 1.3$, which was a value frequently employed in forming diodes. The thermal profile is shown in Figure 24. The liquid-solid interface may

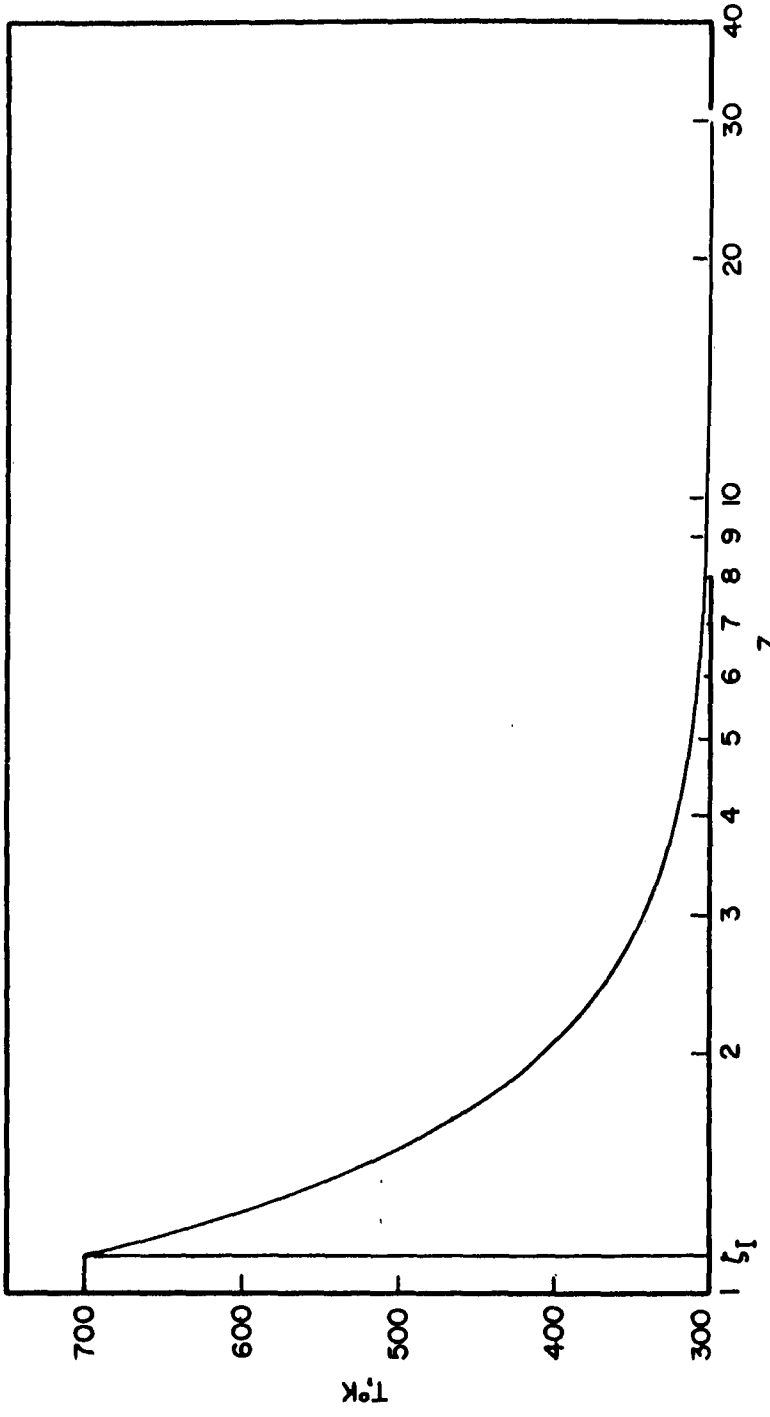

FIGURE 24 TEMPERATURE PROFILE FOR $V_o = 1.3v$. ζ_I = SOLID LIQUID INTERFACE.

be taken to be the surface for which $T(\zeta) = 700^{\circ}K$, the eutectic temperature for the germanium, and corresponds to $\zeta = 1.2$.

It might be noted that the Thompson heating is negligible in comparison to the joule heating except in the region immediately adjacent to the interface, where the high values of T and $dT/d\zeta$ cause it to rise to 20 per cent of the I^2R term.

It is often of interest to be able to calculate the thermal time constant of a structure of this sort. Actually, there are two thermal time constants in a system of this type. The first time constant is the length of time after the application of a voltage which would be required to reach the steady state temperature corresponding to that voltage, assuming that the initial rate of change of temperature were held constant. The second time constant is the length of time after the removal of a voltage for the temperature to return to the ambient temperature, providing that the rate of decrease of temperature remained equal to what it was immediately after the removal of the voltage. For most practical purposes we may regard the two thermal time constants as equal, at least to within an order of magnitude.

To see why this is so, let us first agree to ignore the Thompson heating, an approximation which we have seen should cause an error of 20 per cent or less. Then we may divide the heat flow into two portions: that due to the thermal gradient and that due to the ohmic power loss. Let us call the former Q_T and the latter Q_I. Then:

$$Q_I = \frac{4V_o^2\sigma_s}{\pi^2 a^2(\xi^2+\zeta^2)(1+\zeta^2)} \tag{63}$$

and

$$Q_T = \nabla \cdot (k\nabla T) \tag{64}$$

Before equilibrium is established, the thermal continuity equation must contain a time-dependent term:

$$Q_T + Q_I = C \frac{\partial T}{\partial t} \tag{65}$$

where C is the specific heat of the material.

Suppose now that at time $t = t_a$ we apply a voltage pulse to a "cold" diode. Since, initially, T = the ambient temperature throughout, Q_T is identically zero. Q_T, however, is independent of temperature (as we showed in II) and hence of time, provided only that the applied voltage does not vary. Thus,

$$Q_T + Q_I = \frac{4V_o^2\sigma_s}{\pi^2 a^2(\xi^2+\zeta^2)(1+\zeta^2)} = C \left.\frac{\partial T}{dt}\right|_{t = t_a} . \tag{66}$$

Then the thermal time constant relating to heating up, which we shall call t_1, is

$$t_1 = \frac{T_f}{\partial T/\partial t\big|_{t=t_a}} = \frac{T_f C(\pi^2 a^2)(\xi^2+\zeta^2)(1+\zeta^2)}{4V_o^2\sigma_s} . \tag{67}$$

Here T_f is the final, steady-state temperature. When a steady-state has been reached $Q_T = -Q_I$ and the time derivative is zero. When the voltage is removed, Q_I becomes identically zero and Q_I does not change instantaneously, since the temperature

does not change instantaneously at any point. Hence, if the voltage is removed at $t = t_b$,

$$Q_{T'} + Q_I = Q_T = -Q_I = -\frac{4V_o^2\sigma_s}{\pi^2 a^2(\xi^2+\zeta^2)} = C\frac{\partial T}{\partial t}\Bigg|_{t=t_b} \tag{68}$$

and, defining the cooling-down time constant as t_2

$$t_2 = \frac{T_f C(\pi^2 a^2)(\xi^2+\zeta^2)(1+\zeta^2)}{4V_o^2\sigma_s}$$

C is independent of temperature in the temperature range of interest here, and so is σ_s. Hence $t_2 = t_1$. If Thompson heating were taken into account, it would be a factor in t_1 but not in t_2.

To get some idea of the order of magnitude of t_2, let us take the thermal time constant relating to the solid-liquid interface in the case where $a = 10^{-3}$ cm, $V_o = 1.3$V, $T_f = 700^oK$, $\sigma_s = 10^3$, $\xi = 1$, and $\zeta = 1.2$. C = 5.47 calories/mole or 1.68 joules/c.c. For these values $t_2 = 8.3$ μsec.

This is a quantity which one may check experimentally. Suppose that we have a configuration with a particular value of a, and we apply a pulse of height sufficient to form a good diode, but with a length which is close to the thermal time constant. Then we may expect that, whatever the I-V characteristic of the resulting diode might be, a second pulse of the same length will alter it. If, however, a pulse is applied which is long compared to the thermal time constant, the I-V characteristic should remain

relatively constant with succeeding pulses, presuming that no additional factors such as solid state diffusion enter the picture.

In the experiment a point was lightly performed to a freshly cleaved germanium wafer in such a manner that $a \approx 10^{-3}$ cm (the technique for accomplishing this will be discussed in Section VI). The current at $V_F = 400$ mv was taken as a measure of the I-V characteristic. This quantity is plotted against the number of pulses for various pulse lengths in Figure 25. The wire was torn loose from the semiconductor before each run. Note that, for a pulse length of 6.5 μsec, the value of I_{400} changes considerably from one pulse to the next, whereas for the pulses long compared to the predicted time constant, the variation was slight.

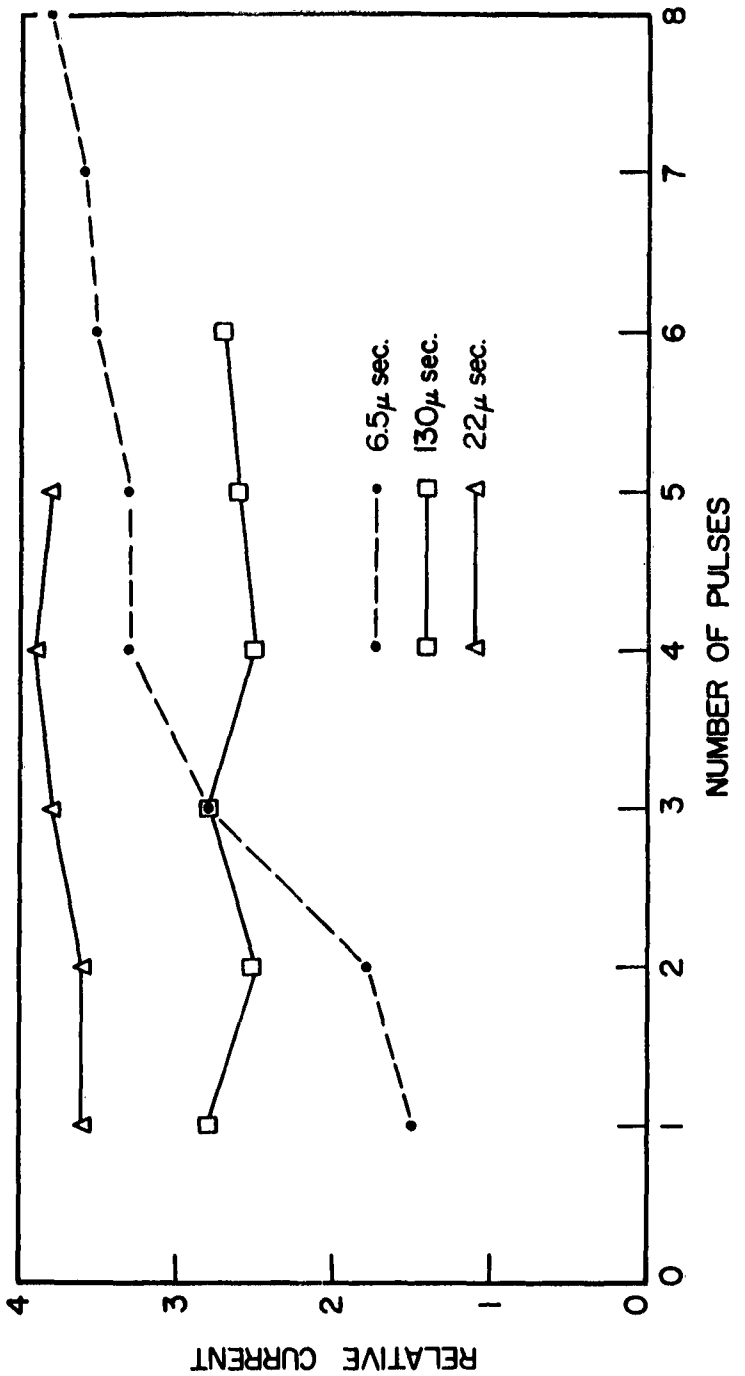

FIGURE 25 RELATIVE CURRENT VERSUS NUMBER OF PULSES.

VI. FACTORS INFLUENCING JUNCTION AREA

There are three factors effecting the junction area: the pressure on the wire, the geometry of the tip of the wire, and the pulse supply impedance.

It is, of course, impossible to touch the wire to the semiconductor and still have zero force upon it. Assuming then that the wire is bearing down on the semiconductor with some nonzero force, and that a pulse of sufficient length from a source of nonzero impedance is applied, the tip of the wire melts, spreads out, and permits more current to flow. Assuming that the pulse is of sufficient duration, this continues until one of two things happens: either the IR drop in the pulse supply causes the applied voltage to fall below the critical value, or enough of the wire melts to release the downward pressure. In the former case, we are left with the aluminum or other point material spread out over the surface, while in the latter the voltage is high enough to cause the formation of a rather extensive alloy region beneath the point extending into the body of the semiconductor.

We shall see in the next section that the latter situation may be expected to lead to good tunneling junctions. It follows from this that, even with supplies of moderately high impedance, we should be able to obtain tunnel diodes, providing that the area

of the contact is small enough. It also follows that, for a given precontact point geometry, the allowable source impedance goes up as the contact pressure goes down.

This was checked experimentally and found to be true. Wires were brought in to contact with the crystal at pressures and with point geometries which normally required 0.1 ohm pulse sources to yield tunnel diodes. It was tacked by means of a 100-1000 ohm source, with pulse lengths sufficient to cause the initial current level of the (non-tunnel) diode to reach some arbitrary level. The portion of the fixture holding the wire was then moved backwards some amount determined by trial and error and dependent upon the amount of springiness in the wire: usually between 0.0001" and 0.001". A pulse from a source having an impedance of between 1 and 100 ohms was applied, and usable tunnel diodes of relatively low peak currents but good peak-to-valley ratios were obtained. (Figure 26). Without this backing-off process, which of course reduced the pressure on the contact, pulses of this impedance level rarely formed good tunnel diodes. Needless to say, if the wire is backed off too much, the forming pulse simply causes the diode to open, or else the very delicate tacked-on contact breaks before pulsing. The permissible impedance of the pulse supply may also be raised by taking extreme care to make the initial contact as light as possible.

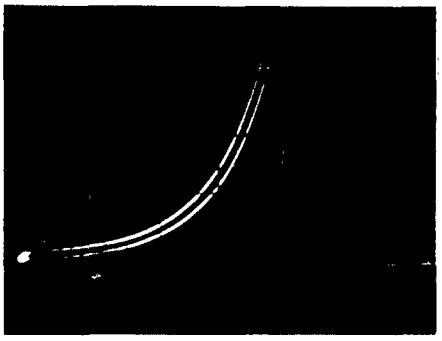

(a)

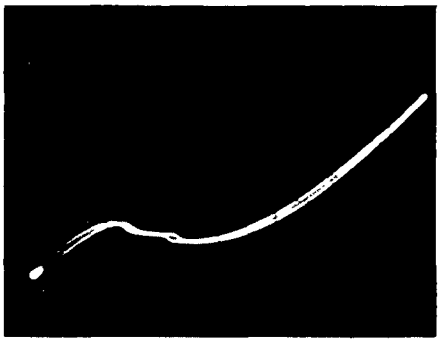

(b)

FIGURE 26 EFFECT OF HEAVY PRESSURE (A) AND LIGHT PRESSURE (B) IN THE FORMING OF DIODES WITH THE SAME INITIAL JUNCTION AREA. IN BOTH CASES, FORMING PULSE WAS 3.0 VOLTS, 10 OHMS, AND 130 MICROSECONDS.

VII. THE IMPURITY PROFILE OF THE FINISHED DIODE

The theoretical and experimental results up to this point have suggested two main types of diode structures. The first type, illustrated in Figure 14, is characterized by a metal-semiconductor surface. This type, typically resulting from high-impedance forming network as described in Section VII, will henceforth be referred to as planar configuration. The second type, which we shall term a spheroidal type, is exemplified by the diode depicted in Figure 18 and Figure 24. It is characterized by a region of metal-semiconductor eutectic extending down into the body of the semiconductor and upwards into the wire.

This latter picture of the diode is substantiated by examination of the regions left when the wire was pulled away after forming. (Figure 11). Ignoring the shear area on the periphery (presumably due to thermal strains set up in the germanium lattice), the area where the wire was pulled away appears to be a smooth spheroidal surface. Estimates of its proportions in the x-direction were possible because of the narrow depth of field of the metallographic objective. By calibrating the amount of motion needed to focus first at the base of the hemispheroid, then on its top, a z-dimension extending above the surface of the semiconductor somewhat less than half the radius of the contact was found. The base of the spheroid was somewhat less than this distance below the surface. This is roughly what we would expect if the surface were the eutectic-aluminum interface. Because of the differential expansion upon cooling between eutectic and aluminum, and possible also because of a difference in lattice configuration, this

interface is very likely a stress concentration plane, and might very well be the first place to fail when the wire is pulled away.

It has been the experience of the Bell Laboratories group (2, 13, 14), as well as our own experience, that low-impedance pulse supplies (which we have seen lead to spheroidal configurations) are necessary to form tunnel diodes. We are now in a position to explain, at least qualitatively, why this should be so.

It was mentioned earlier that diodes of this sort depended upon a process similar to dot-alloy diodes for junction formation. Let us now examine this notion a little more closely.

Alloy junctions (59) are based upon the principle that, when a melt consisting of a semiconductor and a dopant metal cools in contact with germanium, it is possible for the germanium to regrow expitaxially on the solid germanium, incorporating within it small quantities of the dopant metal. The alloy-semiconductor combination in a dot-alloy unit cools by two mechanisms: conduction through to semiconductor to a heat sink, and convection and radiation from the metal. The former ordinarily dominates the latter, although sometimes auxiliary heaters above the wafer are recommended to further slow down the cooling of the top of the melt. If the rate of cooling of the external part of the melt begins to become comparable to that of the allow-semiconductor interface, a situation can result in which nucleation of the regrowing germanium takes place first at point jutting into the alloy. This leads to a jagged junction and often poor diode characteristics.

With a point contact diode, the situation is even worse with respect to the formation of high-quality p-n junctions. Here the portion of

the melt away from the germanium is connected to the point, which is a heat sink having a thermal conductivity many times that of the semiconductor. Thus, in a planar type diode, the thin molten region faces two parallel heat paths, the one corresponding to the point having a far higher thermal conductance than that corresponding to the semiconductor. Under these conditions it is to be expected that the nucleation will take place from the outside in, with little or no nucleation onto the solid germanium, the germanium rejected by the cooling alloy being precipitated in isolated inclusions. Under these conditions the resulting diode will be a poor-quality metal-semiconductor type. This has indeed been the case whenever diodes have been pulsed from the high-impedance sources which we have seen encourage the planar configuration.

The situation which prevails in the case of a pronounced spheroidal configuration such as that found in Section V is considerably more favorable to junction formation. Here the thermal resistance which the alloy-semiconductor interface sees is that of the alloy between the interface and the wire.

To see the importance of this effect let us calculate the thermal resistance looking in both directions from the interface. For our purposes, we may achieve sufficient accuracy by assuming the thermal conductivities of the semiconductor and the alloy are independent of temperature and equal to K_s and K_a, respectively. Let ζ_I = the value of ζ corresponding to the interface, and ΔT_s = the temperature difference between the junction and the ambient

(T(∞)). Then, solving Equation (24) with T substituted for V and K_s substituted for σ_s, we get

$$T = \frac{\Delta T_s}{1 - \frac{2}{\pi}\tan^{-1}\zeta_I} \left[1 - 2/\pi \tan^{-1} \zeta\right] + T \text{ ambient} . \quad (70)$$

The heat flow away from the junction will be

$$H_{ss} = \int_{\substack{\text{area of} \\ \text{junction}}} K_s \nabla T \, da = \frac{2\Delta T_s K_s}{\pi a(1 - \frac{2}{\pi}\tan^{-1}\zeta_I)} \int_{\substack{\text{area of} \\ \text{junction}}} \frac{da}{\sqrt{(\xi^2+\zeta_I^2)(1+\zeta_I^2)}} . \quad (71)$$

The germanium aluminum eutectic is 70 per cent aluminum, so we would expect the alloy to project above the plane of the semiconductor. However, as a conservative estimate let us assume that the alloy-aluminum interface lies at $\zeta = 0$. Then, assuming that we have a planar heat source of temperature ΔT_s + T ambient at $\zeta = \zeta_I$ and that the alloy-aluminum interface is at the ambient temperature,

$$T = T \text{ ambient} + \frac{\Delta T_s}{\text{Tan}^{-1}\zeta_I} \tan^{-1} \zeta \quad . \quad (72)$$

Then the heat flow away from the junction in the direction of the aluminum is then

$$H_{as} = \int_{\substack{\text{area of} \\ \text{junction}}} K_a \nabla T \, da = \frac{\Delta T_s K_a}{a\text{Tan}^{-1}\zeta_I} \int_{\substack{\text{area of} \\ \text{junction}}} \frac{da}{(\xi^2+\zeta_I^2)(1+\zeta_I^2)} \quad (73)$$

and the ratio of the thermal resistivities is

$$\frac{R_s}{R_a} = \frac{\dfrac{\Delta T_s K_a}{a \tan^{-1}\zeta_I}}{\dfrac{2\Delta T_s K_s}{\pi a(1 - \frac{2}{\pi}\tan^{-1}\zeta_I)}} = \frac{K_a \pi(1 - \frac{2}{\pi}\tan^{-1}\zeta_I)}{2K_s \tan^{-1}\zeta_I} . \quad (74)$$

In a planar structure $\zeta_I \rightarrow 0$ and the ratio of resistances becomes infinite. Hence, if we take an electrical analogue and picture the layer of molten eutectic at the alloy-semiconductor interface as a charged capacitor, most of the heat will flow towards the wire, and we would expect the portion nearest the wire to cool down first.

On the other hand, if we cite our example of part V for a heavily formed diode, $\zeta_I \approx 1$ and:

$$\frac{R_s}{R_a} \approx \frac{K_a}{K_s} . \quad (75)$$

The alloy, being a highly disordered structure, will ordinarily have a considerably lower thermal conductivity than the semiconductor, hence $R_s < R_a$, an appreciable quantity of heat flows through the semiconductor and the heat of fusion of a layer of eutectic will have had time to have been removed from a layer bounding the semiconductor before the freezing front from the aluminum side has traversed the melt, and good regrowth and usable tunnel diodes are the result.

The objection might be raised that initial thermal gradients were ignored in this analysis. However, this also was a conservative approximation, since initially the alloy-semiconductor interface looks at a steep thermal gradient in the semiconductor direction and no gradient at all in the alloy direction (the whole melt is presumed to be at the eutectic temperature).

At this stage it might be well to mention very briefly solid state diffusion of the point material into the unmelted crystal.

The diffusion constant D which relates the flux of dopant atoms to the concentration gradient is characterized by a multiplicative constant D_o and an activation energy ΔH.

$$D = D_o \exp\left[\Delta H/RT\right] \tag{76}$$

where R is the gas constant. For aluminum in germanium, there appears to be no data on ΔH on D_o. To get an idea of the order of magnitude of the effect at the temperature which we used in the example, we shall average the values of the neighboring column III elements in germanium (one should, however, have no illusions regarding the validity of such a procedure). This yields $\Delta H \approx 80$ kilocalories and $D_o = 1000\ cm^2/sec$. At $T = 700^oK$, this means D is on the order of magnitude of 10^{-18}. If we ignore the curvature of the interface, we get for the gradient distribution

$$N(+,\ z) = N_I\ \text{erfc}\ \frac{x}{2\sqrt{D+1}} \tag{77}$$

where N is dopant density, N_I is the density at the interface (assumed constant) and t is the time from the application of heat. The solid solubility of aluminum in germanium is about 10^{20} atoms/cc. If we are interested in the period necessary for an appreciable number (say 10^{18}/cc) of dopant atoms to diffuse 100 Angstroms, then we derive a value of t equal to 10^9 seconds. With all due account of the inadequacy of our estimates of ΔH and D_o, it seems unlikely that pulsing formats of less than a second will give rise to solid-state diffusion effects at these temperatures.

VIII. CONCLUSIONS

Before stating the conclusions reached, it might be well to mention some factors which were not considered in this study.

First, we considered a range of dopants and temperatures where intrinsic conduction was never important. However, it is quite possible that this assumption would be invalid in the case of backward diodes and some tunnel diodes.

It was always assumed that electrons, when they were scattered, had their momentum completely randomized. However, it is possible that with the extremely high fields which exist in the neighborhood of the point, "hot electrons" might play some role in transport processes.

The motion of ionized impurity atoms under the influence of high electric fields and high temperatures has received some attention in recent years and might play some role in determining the impurity profile. Unfortunately, certain experimental advantages have caused most of the work in this area to be carried out with lithium as the diffusant, which makes quantitative work with III-V dopants difficult.

Peltier heating, which received little more than a passing mention here since it took place on the alloy side of the junction, might be important in diodes which are reversed pulsed.

Interaction between dopants was ignored; it was assumed that the diffusion of aluminum into the arsenic-doped material dominated the converse process because of the very much higher concentration of aluminum. For an argument which indicates that this might not be the case, the reader is referred to the article by McCaldin (61).

Enumerated below are the contributions which the author feels this work has made to the literature of electrical engineering.

1) It was shown that the rather simple model used by Sim (1) and Torrey and Whitmer (3) was adequate to give accurate numerical estimates of the minimum voltage necessary to give any forming effect, provided that one takes into account the temperature variation of thermal conductivity and the current limiting effect of the metal-semiconductor junction. This is the first and only study of forming which takes these two factors into account.

2) The thermoelectric power, Thompson coefficient, and resistivity of extremely degenerate germanium at elevated temperatures was calculated. Although the computation was straightforward and involved well-known techniques, the parameters for this degree of doping and range of temperatures have not previously been reported in the literature.

3) It is shown that thermoelectric effects can indeed be a significant factor in forming.

4) It is shown that a simple planar model of the sort used by previous investigators does not lead to a situation in which single-crystal regrowth (which a considerable number of thermoelectric probing experiments have indicated occurs) is possible. A model of the forming process in which a alloy region extends into the body of the semiconductor is developed, and fits well with relevant experimental data. In particular, the thermal time constant predicted by the theory appears to be essentially correct, and the configuration of the contact after the point is torn away, which might otherwise be somewhat puzzling, fits directly into the model. Furthermore, it is shown that this picture leads to a heat flow pattern in which conditions for satisfactory regrowth are met. The prediction of this theory, namely that a low impedance pulse supply is necessary for good diode forming, agrees with our own observations and those of other workers in the field.

5) Finally, it is shown that, at least under a rather typical set of conditions, solid state diffusion may be ignored entirely, unless forming times are exceedingly long. This also agrees with empirical observation.

BIBLIOGRAPHY

1. Sim, A. C., "A Quantitative Theory of the Electroformation of Metal-Germanium Point Contacts," Electronic Communications, Vol. 3, p. 139, August 1957.

2. Burris, C. and Tramburolo, R., (Private Conversation).

3. Torrey, H. C. and Whitmer, C. A., Crystal Rectifiers, McGraw-Hill Book Co., Inc., New York, 1948.

4. Valdes, L. B., "Transistor Forming Effects in N-Type Ge.," Proc. IRE, Vol. 40, p. 445, April 1962.

5. Forster, J. H., and Miller, L. E., "The Effect of Surface Treatments on Point-Contact Transistor Characteristics," Bell System Technical Journal, Vol. XXXV, No. 4, p. 767, July 1956.

6. Longini, R. L., "Electric Forming of n-Germanium Transistors Using Donor Alloy Contacts," Physical Review, Vol. 84, p. 1254, 1951.

7. Stelmak, J. P., "Electric Forming of n-Germanium Transistors Using Phosphorous - Alloy Contacts, Physical Review, Vol. 83, p. 165, 1951.

8. Claussen, B. H., "The Influence of Surface Properties on the Characteristics of Formed Point Contacts on P-Type Germanium," The Institution of Electrical Engineers, Supplement B, No. 2935B, p. 282, May 1958.

9. Ebhardt, R., Hofmeister, E. and Groshwitz, E., "Charakteristik Formeirter Spitzingleichrichter," Zeitschrift für Angewandte Physik, Vol. 30, p. 16, 1961.

10. Esaki, L., "Properties of Heavily-Doped Germanium and Narrow P-N Junctions," Solid State Physics in Electronics and Telecommunications, Edited by Deserant, M. and Michels, J., Academic Press, New York, 1960.

11. Lesk, I. A., Holonyok, N., Davidsohn, U. S., and Aarons, M. W., "Germanium and Silicon Tunnel Diodes-Design, Operation, and Uses," IRE Wescon Convention Record, p. 9, August 1959.

12. Sawyer, D. E., "Microprobing of Functioning Semiconductor Devices for Internal Voltage and Current Distributions, Solid-State Electronics, Vol. 5, p. 89, 1962.

13. Burris, C. A., "Gallium Arsenide Tunnel Diodes for High Frequency Applications," Journal of Applied Physics, Vol. 32, No. 6, p. 1031, June 1961.

14. Burris, C. A., "Germanium and Silicon High Frequency Esaki Diodes," Proceedings of the IRE, Vol. 50, No. 7, p. 1689, July 1962.

15. Abeles, B., "Thermal Conductivity of Germanium in the Temperature Range 300°K to 1040°K, Journal of the Physical Chemistry of Solids, Vol. 8, pp. 340-343, 1959.

16. Slack, G. A. and Glassbrenner, C., "Thermal Conductivity of Germanium from 3°K to 1020°K," Physical Review, Vol. 120, No. 3, pp. 782-789, November 1960.

17. Klemens, P. G., "Thermal Conductivity in Lattice Vibrational Modes," Solid State Physics, Advances in Research and Applications, Vol. VII, edited by Seitz, F. and Turnbull, D., Academic Press, New York, 1958.

18. Born, M. and Goeppert-Mayer, M. in Handbuch Der Physik, Vol. 2412, p. 623, Springer, Berlin, 1933, Quoted in Klemens, op. cit.

19. Debye, P. in Vortraege ueber die Kinetische Theorie, der Materie and Electrizitat, Teubner, Berlin, 1914, cited Klemens, op. cit.

20. Callaway, J., "Model for Lattice Thermal Conductivity at Low Temperatures," Physical Review, Vol. 113, p. 1046, 1959.

21. Klemens, P. G., "The Scattering of Low-Frequency Lattice Waves by Static Imperfections," Proceedings of the Physical Society of London, A68, p. 1113, 1955.

22. Trumbore, F. A. and Tartaglia, A. A., "Resistivities and Hole Mobilities in Very Heavily Doped Germanium," Journal of Applied Physics, Vol. 29, No. 10, p. 1511, October 1958.

23. Smith, R. A., Wave Mechanics of Crystalline Solids, John Wiley and Sons, Inc., New York 1961.

24. Price, P. J., "Electronic Thermal Conduction in Semiconductors," Physical Review, Vol. 95, p. 596, July 15, 1954.

25. Price, P. J., "Ambipolar Thermodiffusion of Electrons and Holes in Semiconductors," Philosophical Magazine, Vol. 46, p. 1252, 1955.

26. Morin, F. J., and Maito, J. P., "Conductivity and Hall Effect in the Intrinsic Range of Germanium," Physical Review, Vol. 94, No. 6, pp. 1525-1529.

27. MacFarlane, G. G., McLean, T. P., Quarrington, J. E. and Roberts, V., "Fine Structure in the Absorption-Edge Spectrum of Ge., Physical Review, Vol. 108, p. 1377, 1957.

28. Gaertner, W., "Temperature Dependence of Carrier Densities, Mobilities, Diffusion Constants and Conductivities in Germanium and Silicon," Semiconductor Products, p. 29, July 1960.

29. Brody, T. P., "Nature of the Valley Current in Tunnel Diodes," Journal of Applied Physics, Vol. 33, No. 1, pp. 100-111, (1961).

30. Trumbore, I. A., "Effect of P-Type GeAs Occlusions on the Resistivity of Heavily Doped N-Type Ge", Journal of the Electro-Chemical Society, Vol. 107, p. 198 C(A), August 1960.

31. Morin, F. J., and Maito, J. P., "Conductivity and Hall Effect in the Intrinsic Range of Germanium," Physical Review, VI, 94, No. 6, pp. 1525-1529.

32. Debye, P. P. and Convell, E. M., "Electrical Properties of N-Type Germanium," Physical Review, Vol. 93, No. 4, February 15, 1954, pp. 693-706.

33. Morin, F. J., "Lattice-Scattering Mobility of Germanium," Physical Review, Vol. 62, No. 1, pp. 62-65, January 1954.

34. Bardeen, J. and Shockley, W., "Deformation Potentials and Mobilities in Non-Polar Crystals," Physical Review, Vol. 80, No. 1, October 1, 1950, pp. 62-70.

35. Shockley, W., "Electrons and Holes in Semiconductors," Princeton, D. Van Nostrand and Co., Inc. 1960.

36. Conwell, E. and Weiskopf, V. F., "Theory of Impurity Scattering in Semiconductors," Physical Review, Vol. 77, pp. 388-390, 1950.

37. Conwell, E., "Properties of Silicon and Germanium," Proceedings of the IRE, Vol. 40, pp. 1327-1322, November 1962.

38. Brooks, H., "Scattering by Ionized Impurities in Semiconductors, Physical Review, Vol. 33, No. 4, p. 879, August 1951.

39. Johnson, V. A., and Lark-Horovitz, K., "The Combination of Resistivities in Semiconductors," Physical Review, Vol. 82, No. 6, p. 977, 1951.

40. Hanney, N. B., Semiconductors, Rheinhold, New York, 1959.

41. Brooks, H., "Scattering by Ionized Impurities in Semi-Conductors," Physical Review, Vol. 83, p. 879, 1951.

42. Melnik, V. G., and Gutin, S. S., "On the P-N Junction in Solid Point-Contact Rectifiers," Doklady Nauk S.S.S.R., Vol. 121, pp. 852-4, 1958.

43. Kane, E. O., "Theory of Tunneling," Journal of Applied Physics, Vol. 32, No. 1, p. 83, January 1961.

44. Price, P. J. and Radcliff, J. M., "Esaki Tunneling," I. B. M. Journal of Research and Development, p. 364, October 1959.

45. Fredkin, D. R. and Wannier, G. H., "Theory of Electron Tunneling in Semiconductor Junctions," Physical Review, Vol. 128, No. 5, p. 2054, December 1962.

46. Brody, T. P., "Nature of the Valley Current in Tunnel Diodes," Journal of Applied Physics, Vol. 33, No. 1, January 1962.

47. Franz, W., "Theorie des Rein Elektrischen Durchschlag Fester Isolatoren," Ergebnisse der Exakten Naturwissenschaften, Springer, Berlin, 1953.

48. Spenke, Eberhard, "Electronic Semiconductors," McGraw-Hill Book Co., Inc., New York, 1958.

49. Shockley, W., "The Theory of P-N Junctions in Semi-Conductors and P-N Junction Transistors," Bell System Technical Journal, Vol. 28, No. 3, pp. 435-489.

50. Lockwood, H. F., "Peak Current Behavior in Ge Esaki Junctions," Journal of Applied Physics, Vol. 33, No. 1, p. 245, January 1962.

51. Johsher, A. K., "Principles of Semiconductor Device Operation, Wiley and Sons, New York, 1960.

52. Hohn, R., Electrical Contacts, Stockholm, Almquist and Wiksells, 1946.

53. Mondolphi, L. F., Metalography of Aluminum Alloys, John Wiley and Sons, New York 1943.

54. Tanc, J., "Photo and Thermoelectric Effects in Semi-conductors," Pergamon Press, New York 1962.

55. Johnson, V. A., "Theory of the Seebeek Effect in Semi-Conductors," Progress in Semiconductors, J. Wiley and Sons, New York, 1956.

56. Johnson, V. A., and Lark-Horovitz, K., "Theory of Thermoelectric Power in Semiconductors with Applications to Germanium," Physical Review, Vol. 92, p. 226, October 1953.

57. Middleton, A. E. and Scanlon, W. W., "Measurements of the Thermoelectric Power of Germanium at Temperatures above 78°K", Physical Review, Vol. 92, p. 219, 1953.

58. Blakemore, J. S., "The Fermi Level in Germanium at High Temperatures," Proc. Phys. Soc., 71, 692-4, 1958.

59. Peterson, J. W., McGlasson, J., and Hittinger, W. C., "Some Aspects of Alloying onto Germanium Surfaces," Journal of Metals, Vol. 9, pp. 823-27, July 1957.

60. Pell, E. M., "Ion Drift in an N-P Junctions," Journal of Applied Physics, Vol. 31, No. 2, p. 292.

61. McCaldin, J. O., "Interaction Between Arsenic and Aluminum in Germanium," Journal of Applied Physics, Vol. 31, No. 1.

10 Defense Document Center
Arlington Hall Station
Arlington 12, Virginia

ASD
Wright-Patterson AFB, Ohio
1 Attn: ASAPRL
1 ASAPT
1 ASNC
1 ASND
1 ASNG
1 ASNPVD-1
1 ASNPVD-2
1 ASNR
1 ASNS
1 ASNSED
1 ASNY
1 ASORR (Mr. Catanzarite)
1 ASRC
1 ASRE
1 ASRNET-3
1 ASRNGE
1 ASRNOO
1 ASRNC (Mr. Stimmel)
1 ASRNC (Mr. Portune)
2 ASRNCC-1
1 ASRNCC-2
1 ASRNET-1
2 ASRNCF-1
1 ASRNRS
1 ASRNRS-3
1 ASROO
1 ASRSSE-2
1 ASOQ (Gp. Capt. Fletcher)

1 ARL
Wright-Patterson AFB, Ohio
Attn: ARM (Mr. Wolaver)

RADC
Griffiss AFB, New York
1 Attn: RAAL
1 RAD (Dr. I. J. Gabelman)
1 RALC (J. E. Gruickshank)
1 RALSS (M. A. Diab)
1 RAUAA (John P. Huss)
1 RAUAT
1 RAUMA (C. R. Miller)
1 RAUMM
5 RAWE
1 RAWEC
1 RAWES
2 RAWI

AFSC
Andrews AFB
Washington 25, D.C.
1 Attn: SCTAN
1 SCRC (Lt. Col. Thompson)

HQ, USAF
Washington 25, D.C.
1 Attn: AFRDR-IN (Lt. Col. Pinson)
1 AFOOR-SV-ES (Lt. Col. Smith)
1 AFORQ-SA (Lt. Col. Ragsdale)
1 AFMPP-EQ (Lt. Col. Manbeck)
1 AFORQ-AD

1 USAFSS (ODC-R)
San Antonio, Texas

1 RTD (RTHR, Col. Schulte)
Bolling AFB,
Washington, D.C.

2 PACAF (PFOOT-D)
APO 953
San Francisco, California

2 USAFE (DCS/Ops)
APO 633
New York, New York

1 35 35th NTW
Attn: Electronic Warfare Familiarization Course
Mather AFB, Calif.

1 TAC (OA)
Langley AFB, Va.

1 DCAS (DCLMT/TDC)
AF Unit Post Office
Los Angeles 45, Calif.

SAC
Offutt AFB, Nebr.
1 Attn: DORQP
1 DOPLT

1 AFMDC (MDRRF-1)
Holloman AFB, N.M.

1 Air University Library (AUL-6234)
Maxwell AFB, Ala.

2 9th AF (DOTR-FR (Capt. O.E. McCain)
Shaw AFB, S. C.

1 ADC (ADOOA)
Ent AFB, Colorado

1 Director
Weapons Systems Evaluation Group
Room 1E-875, The Pentagon
Washington 25, D.C.

10 Scientific and Technical Information Facility
Attn: NASA Representative (Code: S-AK/DL)
P. O. Box 5700
Bethesda, Md.

1 Commanding Officer
U.S. Army Signal Res. and Dev. Lab.
Attn: SIGRA/SL-SE, Mr. I. O. Myers
Fort Monmouth, N.J.

1 Chief Signal Officer
Research and Development Div.
Avionics and Surveillance Branch
Washington 25, D.C.

1 Assistant Secretary of Defense
Research and Development Board
Attn: Technical Library
Department of Defense
Washington 25, D.C.

1 Director
National Security Agency
Attn: C3/TDL
Fort George G. Meade, Md.

1 Army Ordnance Missile Command
Attn: ORDXM-RR, Hallowes, Jr.
Redstone Arsenal, Alabama

2 Commanding General
Army Ordnance Missile Command
Attn: AMSMI/RNR - Re-entry Physics Branch
Redstone Arsenal, Alabama

1 Commanding Officer
U.S. Army Signal Res. and Dev. Lab.
Attn: SIGRA/SL-N-5, Dr. H. Bennett
Fort Monmouth, N.J.

1 Commanding General
White Sands Missile Range
Attn: ORDBS-OM-TL
New Mexico

2 Commanding Officer
Picatinny Arsenal
Attn: Tech. Information Section
ORDBB-VA6
Dover, N.J.

1 USA Signal Electronic Research Unit
P. O. Box 205
Mountain View, Calif.

1 US Army Signal Corps School
Attn: DST, USASCS (Mr. Henry Allem)
Fort Monmouth, N.J.

1 Chief of Naval Research
Attn: Code 427
Department of the Navy
Washington 25, D.C.

1 Commander
U.S. Naval Ordnance Laboratory
Attn: Eva Liberman, Librarian
White Oak, Silver Spring, Md.

1 Director
Material Laboratory
New York Naval Shipyard
Brooklyn 1, N.Y.

1 Commander
U.S. Naval Missile Center
Attn: Technical Library,
Code NO 3022
Point Mugu, California

1 Commanding Officer
U.S. Naval Air Dev. Center
Engineering Development Lab.
Attn: J. M. McGlone
Johnsville, Pa.

1 Commanding Officer
U. S. Naval Ordnance Laboratory
Attn: Code 74
Corona, California

1 Chief
Bureau of Naval Weapons
Department of the Navy
Attn: RRRE-2
Washington 25, D.C.

2 Director
U. S. Naval Research Lab.
Attn: Code 2027
Washington 25, D.C.

1 Chief, Bureau of Ships
Attn: Code 335
Room 1532, Main Navy Building
18th and Constitution Ave., N.W.
Washington 25, D.C.

1 Airborne Instruments Lab.
A Division of Cutler-Hammer Inc.
Attn: Library
Walt Whitman Road
Melville, Long Island, N.Y.

1 Analytic Services, Inc.
Attn: Library
1150 Leesburg Pike
Bailey's Crossroads, Va.

2 The Johns Hopkins University
Applied Physics Laboratory
Attn: Mr. George L. Seielstad
8621 Georgia Avenue
Silver Spring, Md.

1 Bjorksten Research Labs., Inc.
P. O. Box 265
Madison 1, Wisconsin

1 Cook Electric Company
Cook Technological Center Div.
6401 W. Oakton Street
Morton Grove, Ill.

1 Electronic Communications, Inc.
Research Division
1830 York Road
Timonium, Md.

1 General Dynamics/Fort Worth
A Div. of General Dynamics Corp.
Attn: Chief Librarian
P. O. Box 748
Fort Worth 1, Texas

1 General Electric Company
Advanced Electronics Center
Attn: Library
Cornell University Industrial Res. Park
Ithaca, N.Y.

1 Grumman Aircraft Engineering Corp.
Engineering Library, Plant 5
Attn: M.O. Friedlander, Head Librarian
Bethpage, Long Island, N.Y.

2 The Hallicrafters Company
Attn: Library
4401 West Fifth Avenue
Chicago 24, Illinois

1 HRB-Singer, Inc.
Attn: Library
Science Park Box 60
State College, Pa.

1 The University of Michigan
Institute of Science and Technology
Attn: IRIA
P. O. Box 618
Ann Arbor, Michigan

2 ITT Federal Laboratories
Div. International Telephone and
Telegraph Corp.
500 Washington Avenue
Nutley, N.J.

1 Jansky and Bailey
A Div. of Atlantic Research Corp.
1339 Wisconsin Ave., N.W.
Washington 7, D.C.

1 Massachusetts Institute of Technology
Lincoln Laboratory
Attn: Library
P. O. Box 73
Lexington 73, Mass.

1 Massachusetts Institute of Technology
Electronics Systems Laboratory
Attn: John E. Ward, Rm. 32-101
Cambridge 39, Mass.

1 Lockheed Georgia Company
Attn: Dept. 72-15
Marietta, Ga.

1 Martin-Marietta Corp.
Martin Company Division
Attn: Science-Technology Library
Baltimore 3, Md.

1 Mitre Corp ration
Attn: Libra
Bedford, Mass.

1 Motorola Inc.
Systems Research Lab.
8330 Indiana Avenue
Riverside, Calif.

2 North American Aviation, Inc.
Attn: Technical Library
International Airport
Los Angeles 9, California

1 Northrop Corporation
Norair Division
Attn: Technical Information, 3924-31
1001 E. Broadway
Hawthorne, Calif.

2 Radio Corporation of America
Defense Electronic Products, DSD
Attn: L. R. Hund, Librarian
8500 Balboa Blvd.
Van Nuys, Calif.

1 Raytheon Company
Attn: Librarian
P.O. Box 636
Santa Barbara, Calif.

1 Revere Copper and Brass Inc.
Foil Division
Attn: Mr. Arthur Ferretti
196 Diamond Street
Brooklyn 22, N.Y.

1 Stanford University
Stanford Electronics Labs.
Attn: Security Officer
Stanford, Calif.

1 Sylvania Electric Products Inc.
Technical Information Section
P. O. Box 188
Mountain View, Calif.

1 Sylvania Electric Products, Inc.
Sylvania Electronic Systems
Attn: Applied Research Lab. Library
40 Sylvan Road
Waltham 54, Mass.

1 The Ohio State University
Research Foundation
Attn: Dr. Curt A. Lewis
1314 Kinnear Road
Columbus 12, Ohio

1 The RAND Corporation
Attn: Library
1700 Main Street
Santa Monica, Calif.

1 The University of Michigan
University Research Security Office
Attn: Dr. B. F. Barton
Director, CEL
P. O. Box 622
Ann Arbor, Michigan

2 Thompson Ramo-Wooldridge Inc.
Ramo-Wooldridge Division
Attn: Technical Library
8433 Fallbrook Avenue
Canoga Park, Calif.

1 Space Technology Labs., Inc.
STL Technical Library
Attn: Document Acquisitions Group
One Space Park
Redondo Beach, Calif.

1 Unidynamics
Div. of Universal Match Corp.
Attn: Technical Library
4407 Cook Avenue
St. Louis, Missouri

1 Westinghouse Electric Corporation
Defense Center - Baltimore
Attn: Technical Information Center
P. O. Box 1693
Baltimore 3, Maryland